A new square pyramidal copper(II) complex [Cu(C10H24N4)Br]Br: Crystal structure, thermal analysis, Hirschfeld surfaces, electrical and semiconducting properties

Wassim Maalej, Philippe Guionneau, Zakaria Elaoud

A new square pyramidal copper(II) complex [Cu($C_{10}H_{24}N_4$)Br]Br: crystal structure, thermal analysis, Hirschfeld surfaces, electrical and semiconducting properties.

Wassim MAALEJ[1*], Philippe GUIONNEAU[2] and Zakaria ELAOUD [1]

[1]*Laboratory of Physical and Chemistry of Solid State, University of Sfax, Faculty of Sciences of Sfax, B.P. 1171, 3000 Sfax,Tunisia.*

[2]*CNRS, Univ. Bordeaux, Bordeaux INP, ICMCB, UMR 5026, 87 avenue Dr A. Schweitzer, 33608 Pessac, France*

* Corresponding Author:

Dr. Wassim MAALEJ:
Department of Chemistry,
Laboratory of Physical and Chemistry of Solid State
University of Sfax, Faculty of Sciences of Sfax,
B.P. 1171, 3000 Sfax, Tunisia
E-mail: maalej_wassim@hayoo.fr
maalej.wassim@fsg.rnu.tn

Abstract

A new organic-inorganic Cu(II) bromide complex material [Cu($C_{10}H_{24}N_4$)Br]Br has been synthesized by hydrothermal method. Blue-violet crystals are characterized by X-ray single crystal diffraction, crystallizing in the orthorhombic system, non-centrosymmetric space group $P2_12_12_1$, with the following unit-cell parameters: a = 8.3536 (1) Å, b = 12.7161 (3) Å, c = 14.1982 (3) Å, V = 1508.21 (5) $Å^3$. This study shows that the Cu(II) sites adopt a square pyramidal distorted geometry. The crystal structure first reveals a one-dimensional (1D) network along the *a* axis based on N–H···Br interactions. The dimensionality is further increased to (3D) by C–H···Br weak interactions. Hirshfeld surfaces analysis was used to study the intermolecular interactions in the crystal lattices. It was then found that X-H···Br (X = N or C) contacts play an important role within the atomic architecture. Besides, the phase transitions, electric and optical properties of [Cu($C_{10}H_{24}N_4$)Br]Br were investigated and revealed a phase transition at T=343 K. The temperature dependence of the electrical conductivity confirmed the phase transition that was also well detected with differential scanning calorimetry. The calculated activation energies of the conduction process for the two phases are EaI=0.30 eV, and EaII=0.69 eV.

Keywords: Hydrothermal synthesis, Organic-inorganic, Crystal structure, Optical properties, Phase transitions, Electrical properties, Semiconductor material.

1. Introduction

Nowadays, transition metal complexes are attracting wide attention not only because of their intriguing variety of architectures and molecular topologies [1-5], but also but also these new materials are also sought for improved optical, and electrical properties, magnetic, medicinal, luminescence and ionic conductivity, as well as chemical or biochemical activity [6-17]. A good example among these promising complexes is when Cu(II) is the central metal, since copper complexes have been reported to show versatile properties and applications [18-21]. Moreover, copper(II) is an ideal candidate for the preparation of multinuclear complexes owing to its numerous possibilities of coordination number and geometries which are multiplied by the synergy with the versatility of the ligands. In a general way, the construction of attractive structural topologies immensely depends on the chosen organic ligands and the coordination geometry of central metal ions. In addition, the self-assembly processes are highly sensitive to diverse synthetic conditions and in some cases, the modifications of the reaction conditions such as the solvent, pH and temperature for a given set of organic ligands and metal ions can cause various supramolecular architectures which includes polymorphism [22-24].

Recently, a great effort has been devoted to the self-assembly of organic and inorganic molecules in the solid state, that is, in addition to the coordination bond, non-covalent interactions such as hydrogen bonds, electrostatic interactions and π–π stacking are effective in establishing particular contacts which occur regularly, and play a significant role in driving molecules during crystallization towards desired physical properties. The literature shows that there are many interesting topological structures such as one-dimensional (1D) tapes, two-dimensional (2D) sheets, and three-dimensional (3D) networks which have been built through hydrogen bonding interactions [25-28]. Because of their ubiquitous role in diverse fields, the investigation and understanding of these weak interactions have become one of the major objectives to understand conductive properties and phase transitions in supramolecular chemistry [29,30].

The semiconducting properties of metal(II) halide complexes with hydrogen bonds seem interesting from the viewpoint of crystal engineering. For example, Xiaoqiang Liang et al. [31] studied [Cu(PPA)I] (1) and [$Co(PPA)_2(BDC)(H_2O)_2 \cdot (PPA)_2(H_2BDC)_2(H_2O)$] (2) (PPA= 4-(3-pyridinyl)-2-amino pyrimidine, H_2BDC =1,4-benzenedicarboxylicacid). These two compounds exhibit 0D and 3D strong hydrogen-bonding interactions, respectively. Moreover, their results indicate that conductivities and activation energies of compounds 1 and 2 are 1.64 10^{-4}S cm^{-1}/ 0.19 eV, and 2.29 10^{-4}/ 0.24 eV at 325 K, respectively. The study shows that hydrogen

interactions have a crucial impact on conductivity. The other systems such as $[(TPPB)CuCl_2]_n$ (1),$[[(TMPB)CuCl_2].H_2O]_n$ (2) and $[(TPPB)CuBr_2]_n$ (3), namely 1, 3, 5-tris(2-alkylthiolpyrimidinyl)benzene (alkyl = Et: TPPB TMPB:alkyl = Me; TEPB) [32]. Single crystal X-ray diffraction analysis shows that all 3-D supramolecular architectures form through interactions such as hydrogen bonds. In these crystals, the room temperature dc electrical conductivity of 9.6 10^{-12} S cm^{-1}, 2.9 10^{-9} S cm^{-1} and 2.6 10^{-12} S cm^{-1}, respectively. $[[(TMPB)CuCl_2].H_2O]_n$ (2) displays the highest dc conductivity among others, indicating that their conductive properties heavily depend on C–H···S supramolecular interactions. In addition, researchers are currently focusing on synthesizing metal-organic as an outstanding class of designed crystalline proton conductors. For examples, $[Cu(Hsfpip)(H_2O)_2]\cdot H_2O$, $[CuH_2(Hsfpip)_2(H_2O)]$, $[CuH(Hsfpip)Cl(H_2O)]$ (Hsfpip = 2-(2-(2,4 disulfophenyl)imidazo(4,5-f)(1,10)-phenanthroline) [33]; $\{[Zn(PIP)_2(H_2O)_4]\cdot NDS\}$ and $\{[Ni(PIP)_2(H_2O)_4]\cdot NDS\}$ (PIP = 4-pyridylacrylic acid and NDS = sodium 1,5-naphthalenedisulfonate) [34]; $[Co^{II}Cl_3(H\text{-}MPPA)]$ (H-MPPA = (R)-2-methylpiperazine) [35]. Interestingly, these materials are good proton conductors. It is also worth noting that hydrogen bonding interactions can be considered donor-acceptor systems (the H atom is the acceptor, while N, O, and Cl are donors that provide a lone pair of electrons) to lead to the formation of 3D frameworks. Although some organic metal halide materials with high conductivity in the range of 10^{-4} S cm^{-1} have been observed [33,36].

The interest for the physical properties of the halide complexes is therefore mainly caused by hydrogen bonds [37,38]. Indeed, for example, in the compounds $(C_6H_{14}N)_2SbCl_5$, $(C_6H_{14}N)_2SbBr_5$, $(C_6H_{14}N)_2BiCl_6.H_3O$ and $(C_6H_{14}N)_2BiBr_5$ [39], the hydrogen bonds highly influence the polymeric chain orientation and consequently are one of the reasons for the mechanism of the transitions. The most promising electrical properties have been disclosed for $(C_6H_{14}N)_2SbCl_5$, which exhibits, at temperatures above 333 K, the relatively large electric conductivity of the order of 10^{-6} - 10^{-5}S cm^{-1}characteristic of semiconducting materials. Elsewhere, another hybrid compound, the dimethylammonium manganese (II) formate, $(CD_3)_2ND_2[Mn(DCO_2)_3]$ (Tc~183 K) has been reported to exhibit an order-disorder phase transition in the range of 7-293K linked to short hydrogen bonds [40].

The above observations for the organic metal complexes based on $(C_6H_{14}N)$ urged us to synthesize and characterize the metal bromide compounds. In this paper, we will present the crystal structures, thermal analysis, optical and dielectric properties, spectroscopic and Hirschfield surfaces analysis of the novel Cu(II) bromide complex $[Cu(C_{10}H_{24}N_4)Br]Br$.

2. Experimental section

2.1. Synthesis

The analytical grade chemicals were used without any further purification for the synthesis and were purchased from Aldrich. Crystals of $[Cu(C_{10}H_{24}N_4)Br]Br$ were synthesized and grown by mild hydrothermal method. Copper bromide ($CuBr_2$) (1 mmol) was first dissolved into hydrobromic acid (8 mL), in which 1,4-bis(3-aminopropyl)piperazine (1 mmol) was added in a second step. The mixture of these constituents in a volume of 10 mL of ionized water and 20 mL of acetonitrile was stirred to homogeneity. After that, it was poured into a PTFE-lined stainless steel pressure vessel (fill factor 50%) and heated at 120 °C for 3 days, followed by slow cooling to room temperature. The resultant blue violet crystals with a tall amount retrieved by filtration, washed with methanol and acetone, and finally dried at room temperature. The initial pH of the reaction mixture was approximately 3.5. The purity of the compound was confirmed by an elemental microanalysis: Anal. (Calcd): C, 28.85% (28.34%); H, 6.42% (5.71%); N, 13.73% (13.22%). The reaction scheme of the synthesis is shown below (**Fig.1**)

2.2. *Thermal measurements*

Differential thermal analysis (DTA) and thermogravimetric analysis (TGA) measurements were performed on our heating the sample in a platinum crucible from 300 to 750 K in a SETARAM thermal analyser (TG-ATD92) under air at a heating rate of 5 K min^{-1}.

The differential scanning calorimetric measurements were using a PerkinElmer DSC 4000 instrument. A crystal sample (5.5 mg) was put in aluminium capsule, then heated and cooling starting from 223 to 373 K with a speed rate of 5 K min^{-1}.

2.3. Single crystal structure determination

The single-crystal X-ray diffraction data of $[Cu(C_{10}H_{24}N_4)Br]Br$ crystals were collected at 293 K on an APEX-II Bruker AXS diffractometer and processed with the APEX 2 program suite [41]. The used X-ray wavelength was the Mo-Kα radiation (λ = 0.71073 Å). The frame integration and data reduction were carried out with the program SAINT [42]. The program SADABS [43] was employed for multi-scan-type absorption corrections. The crystal structures were solved by direct methods and dual space methods using the SHELXT software package [44], and refined with full-matrix least-square methods based on F^2(SHELXL) [45] through the WinGX program suite [46]. All non-hydrogen atoms were anisotropically refined, and the positions of H-atoms were geometrically assigned and allowed to ride on their parent atoms, with C–H = 0.97 Å and N–H = 0.89 Å. The software Diamond [47] was used to create the

graphic representations of the crystal structures. Crystallographic data, details on data collections and refinement parameters of the crystal structures are listed in **Table 1**. The hydrogen bonds are listed in **Table 2**. The relevant selected bond lengths and angles are in summarized **Tables S1-S2**, respectively. In order to visualize the intermolecular interactions in the crystal of the title compound [Cu($C_{10}H_{24}N_4$)Br]Br, Hirshfeld surface analysis (Hirshfeld, 1977) [48] was carried out by using CrystalExplorer [49].

Crystallographic data for the structural analysis have been deposited with the Cambridge Crystallographic Data Centre, CCDC No 2060317 and can be obtained via https://www.ccdc.cam.ac.uk/structures.

2.4. Spectroscopic measurements

Infrared measurements were obtained using a Perkin-Elmer FT-IR Spectrum and the samples were diluted with spectroscopic grade KBr and pressed into a pellet. All the bonds were assigned by comparison with the spectrum of other compounds, at room temperature and in the 400–4000 cm^{-1} frequency range. Furthermore, UV–Visible absorption spectra were performed at room temperature, within the range of 200–800 nm, employing a Lambda 1050 UV/Vis/NIR spectrometer. This technique makes it possible to determine the absorbance (A) and the reflectance (R). The optical absorption spectrum of the compound was recorded at room temperature. The powdered crystals of [Cu($C_{10}H_{24}N_4$)Br]Br were used for the measurements.

2.5. Electrical measurements

The real and imaginary parts (Z’ and Z") of impedance were measured on pellet disks of about 8 mm in diameter and 1.1 mm in thickness over the frequency range of 1-10^6 Hz with a SOLARTRON SI 1260 impedance equipment coupled to a dielectric interface in the temperature range of 293–393 K.

3. Results and discussion

3.1 Thermal properties

The thermal analyses (TGA and DTA) were conducted to evaluate the thermal behaviour of the complex, and ascertain the temperature of decomposition. The TGA and DTA curves of the complex are presented in **Fig.S1**. The TG thermogram shows that the compound seems to be stable up to 465 K. Above this temperature, the TGA showed that the decomposition started at 470 K, and continued till 621K. 47.36 % of the sample was lost, which corresponds to the organic molecule bound to Cu(II) (calc: 48.19 %), with two exothermic peaks observed on the

DTA curve at 520 K and 562 K. A similar decomposition has been observed in other hybrid-halide compounds. In addition the hump that has been observed at (≈345.2K) may be attributed to revealing a phase transition. Thereby, one of the best ways to detect whether a compound displays phase transitions triggered by temperature is to perform DSC measurement to confirm the existence of a heat anomaly occurring during the heating and cooling process [50,51]. Therefore, the DSC measurement exhibited a highly remarkable reversible phase transition as shown in **Fig.2**. During the heating and cooling course, [Cu($C_{10}H_{24}N_4$)Br]Br undergoes an hysteretic phase transition by showing a large exothermic peak at 343.2 K and an endothermic peak at 291.1 K. These observed peaks represent a prominent and reversible phase transition with a very large thermal hysteresis of 52.1 K, which is indicative of a first-order phase transition.

3.2 Single crystal structure analysis

In order to understand the details of the structure of [Cu($C_{10}H_{24}N_4$)Br]Br, single-crystal X-ray diffraction data were collected at 293 K. The compound crystallizes in the orthorhombic system, non-centrosymmetric space group $P2_12_12_1$, with the following unit cell dimensions a = 8.3536 (1) Å, b= 12.7161 (3) Å, c = 14.1982 (3) Å, V = 1508.21 (5) $Å^3$. The asymmetric unit consists of one monomeric isolated $[Cu(C_{10}H_{24}N_4)Br]^+$ cation and a free Br^- anions. The crystal atomic architecture is based on a discrete mononuclear packing as depicted in **Fig.3**.

The Cu^{2+} ion is pentacoordinated by the four N-donor atoms (N1, N2, N3 and N4 atoms) of the neutral tetradentate amine, 1,4-bis(3-aminopropyl)piperazineandone bromide atom Br1. The geometry of coordination of the copper (II) centre can be described as a square pyramid distorted geometry towards a trigonal bipyramidal arrangement by a τ value of 0,127. This trigonal index was calculated using the formula $\tau = (\beta - \alpha)/60$ previously defined by Addison et al. [52], with τ assuming the values of 0 or 1 for ideal square-pyramidal and trigonal-bipyramidal geometries. In complex, β and α correspond to N1–Cu–N3 (160.79 (14) °) and to N2–Cu–N4 (153.15 (15) °) angles, respectively.

The equatorial coordination of the Cu(II) centre is composed of four nitrogen atoms from 1,4-bis(3-aminopropyl)piperazine. The Br1 occupies the apical pyramidal position at 2.6028 (6) Å and a deviation of Cu(II) from the basal plane of 0.396 Å. This axial elongation is due to Jahn-Teller effect characteristic of Cu(II) complexes [53,54]. The Cu–N bond lengths are relatively insensitive to ring strain and/or alkyl substitution on the aliphatic linear tetradentate amines. The Cu–N(1), Cu–N(2), Cu–N(3) and Cu–N(4) are 2.062 (4), 2.076 (3), 2.004 (4) and

2.006 (3) (Å), respectively, these lengths are within the expected values of the Cu(II) complexes [55,56]. In the case of the [$C_{10}H_{24}N_4$] ligand, the selected bond lengths and angles fall within the normal ranges. Indeed, the C–C, N–C distances and the C–N–C, N–C–C, C–C–C angles are comparable with those observed in other similar hybrid metal-halide compounds with the same amine ligand [55,57,58].

The crystal lattice in [Cu($C_{10}H_{24}N_4$)Br]Br is stabilized by intramolecular and intermolecular hydrogen bonds (between the N and Br atoms) with N3…Br1 contacts of 3.557 (4) and N4…Br1 of 3.462 (4) Å, and by a combination of weak C–H…X from 1,4-bis(3-aminopropyl)piperazine ligand forming a one dimensional of [Cu($C_{10}H_{24}N_4$)Br]$^+$ cations zig-zag chain (C3–H3B…Br1 and C5–H5B···Br1^{ii}, symmetry codes: (ii) $x-1/2, -y+1/2, -z+1$), are aligned along the [010] direction (**Fig.4**). Copper atoms are stacked one over the other along the three crystallographic axes with a shortest distance Cu···Cu = 6.348 Å which is more than the sum of the van der Waals radii of the copper ions [59]. Hence, there is no metallophilic Cu···Cu interaction in this compound as observed in other similar hybrid [55,56].

The [Cu($C_{10}H_{24}N_4$)Br]$^+$ cations are stabilized by five hydrogen bonds with the uncoordinated bromine anion Br2 is the acceptor. As shown in **Fig.5**, the counter-ions Br^- interacts with nitrogen atoms hydrogen (H33A, H44B) with N···Br distances of 3.411 (6) 3.493 (4) Å respectively N3–H33A…Br2 and N4–H44B…Br2. This cations is further stabilized by the weak C–H···Br2 interactions (C3–H3B···Br2^{iii}, C7–H7B…Br2^{iv} and C10–H10A…Br2^{v}) of the ligand to form another 2D structure (Symmetry code: (iii) $-x+3/2, -y+1, z+1/2$; (iv) $-x+2, y-1/2, -z+1/2$; (v) $-x+5/2, -y+1, z+1/2$).

Medium strong N–H…Br hydrogen bonding which leads to the formation in 1-D zigzagged chains that packs in 3-D supramolecular via weaker C-H...Br hydrogen interactions as shown in **Fig.6**. The details of hydrogen bond interactions are given in **Table 2**.

3.3 Infrared Spectroscopy

FTIR spectroscopy was used to verify the functional groups present in the crystal and to investigate their vibrational behaviour in the solid state. The experimental IR spectrum of the crystalline complex is superimposed in **Fig.7**. The assignment of the characteristic vibrational modes of this compound is mainly based on the theoretical results and on comparison with similar materials [60,61]. In the high frequency domain, the IR spectrum is decomposed in three well separated bands. The first exhibited characteristic absorptions of primary amine at 3338 and 3408 cm^{-1} correspond respectively to the asymmetric and symmetric vibrations of the Ar-

NH_2 [57]. For the ethyl group in aliphatic compound, the asymmetric and symmetric vibrations mode appears in the range 3124-3095 cm^{-1}. The later, band centered at 2890 cm^{-1} attributed to the allylic (CH_2) [62]. At lower frequency range, the intense band at 1600 cm^{-1} are assigned to the deformation of N-H. The asymmetric stretching modes υ_{as}(C-N) for both the type of compounds lie in the region 1464-1300 cm^{-1} for allylic and aliphatic stretching respectively, while the $\upsilon_s(C\text{-}N)_{alip/all}$ vibration are also observed as two peaks same region at 1020-975 cm^{-1}. Moreover, the very strong bands at 1140-1079 cm^{-1} are ascribed to C-C stretching. Finally, the series of bands observed from 950 to 620 cm^{-1} are assigned to the rocking, in-plane deformation and out-of-plane bending of (CH_2), (N-H), C-C-N and C-C-C in the organic skeleton.

Regarding the ligand-to-metal-vibrations, the bands in 544-508 cm^{-1} and 422 cm^{-1} regions may be assigned to υ(Cu-Br) and υ(Cu-N) stretching, respectively. The Cu-N band is observed in the region of 441-550 cm^{-1} [63]. The characteristic IR frequencies (cm^{-1}) of the complex [$CuBr(C_{10}H_{24}N_4)$]Br are shown in **Table S3**.

3.4 Hirshfeld surface

Hirshfeld surface (HS) analysis enables the calculation and the direct visualization of intra and intermolecular interactions by different colours and colour intensity, representing short or long contacts and indicating the relative strength of the interactions. The red regions indicate the contacts shorter than the sum of the van der Walls radii of the involved atoms, while the blue and white regions indicate the contacts longer and closer to the van der Waals limit, respectively. The (HS) and the 2D-fingerprint plots (FP) of the compound [$Cu(C_{10}H_{24}N_4)$Br]Br were generated on the asymmetric unit using the CrystalExplorer program [49]. The crystallographic information file obtained from the single crystal X-ray diffraction analysis was used as input. **Fig.8a** shows the d_{norm} surfaces which were mapped over a scale of -0.2 (red) to 1.4 (blue), to facilitate the visualization of the molecular moiety, transparent surfaces have been illustrated. 2-D fingerprint plots were obtained with the combination of d_i and d_e distances, in the scale of 0.4 to 2.6 Å to summarize the contacts building the crystal structure **Fig.8b**. The d_{norm} HS of the complex shows some deep red spots labelled as 1, 2, 3 and 4, which indicates the presence of short contacts in the crystal structure of the complex, indicating the presence of the non-classical hydrogen bonds C-H…Br, as well as the more classical hydrogen bonds N-H…Br. Also, H…H interactions are observed as small very light-colored spots around the hydrogen atoms zones (labels 5, 6, 7 and 8). The FP plots show the presence of intermolecular contacts H···H and H···Br, corresponding to a high ratio of the

interactions with 69.1% and 30.9% respectively, which revealed that the main intermolecular interactions come from H…H intermolecular contacts. The Br…H interactions were represented by a small area in the top left and bottom right side ($d_i + d_e \approx 2.464$ Å), whereas the H…H interactions were represented by the largest region in the fingerprint plot (**Fig. 8b**) ($d_i + d_e \approx 2.152$ Å) and thus have a most significant contribution to the total Hirshfeld surfaces (69.1%).

3.5 Optical properties

In order to determine the gap energy of the complex, the UV–Vis absorption measurements were carried out up to 800 nm on the crystals sample. The UV–Vis spectrum of $[Cu(C_{10}H_{24}N_4)Br]Br$, is shown in **Fig.9**. The absorption spectrum exhibits two distinct absorption bands which are similar to that observed for other bromo-copper(II) mixed-ligand copper complexes [56,61,64]. The first one, in the ultraviolet region, the complex spectrum displays a strong band at 261 nm is most probably to bromo→Cu (Br_pσ→ Cu_$d_{x^2-y^2}$) ligand to metal charge transfer (LMCT) transition [65,66]. The second one, in the visible domain, a broad band between 480 and 720 nm range arise from d–d transition of Cu(II), which may be taken as evidence for square-pyramidal bromocomplexes. Since the transition may be assigned as the $d_{x^2-y^2} \rightarrow d_{xz}$, d_{yz} and $d_{x^2-y^2} \rightarrow d_{z^2}$ [32,65]. The broadness in the observed band may be attributed to a Jahn-Teller distortion of the geometry with the much-distorted [4 + 1] coordination around the Cu^{2+} cations [56,67]. The Cu–N/Br bond lengths in the range of Cu–N/Br = 2,012 (5) - 2,606 (9) Å. The absorption spectrum of $[Cu(C_{10}H_{24}N_4)Br]Br$ compound displays an intense peak in the ultraviolet spectral region, suggesting a direct band gap [68-70]

To determine the transport properties of this material, we can calculated the gap energy (E_g) from absorption coefficient (α) (1) by means of the Tauc equation (2):

$$\alpha = 2.303A/d \quad (1)$$

$$\alpha h\nu = B(h\nu - E_g)^n \quad (2)$$

where "A" is the absorbance , "d" is the thickness , "Eg" is the band gap, "*h*" is Planck's constant, "ν" is the frequency of light and the exponent "*n*" is the electron transition process-dependent constant. "B" is a constant, which is taken as 1 for ideal case.

To calculate the direct and indirect optical band gap, the value of *n* has been considered as 1/2 and 1, respectively [71]. The dependence of $(\alpha h\upsilon)^2$ and $(\alpha h\upsilon)^{1/2}$ vs $h\nu$ plot in **Fig.10**. The

values of the optical band gap E_g are obtained by extrapolating the linear part of the curve to intersect the X-axis [72]. The estimated band gaps energies are 3.91 and 3.5 eV, for the direct and indirect transitions, respectively. These values clearly classify this material among the semiconductor [73].

3.6 Electrical properties

Impedance spectroscopy measurement was used to characterize the electrical behaviour of this material in which a number of strongly coupled processes exist and to characterize the transition phases detected by the calorimetric study. The variation of the Nyquist plot (-Z" versus Z') of the [Cu($C_{10}H_{24}N_4$)Br]Br carried out from 293 K to 393 K is represented in **Fig.11**. In these curves, the experimental points show two semi-circles where their diameters decrease with increase temperature indicating that the conduction mechanism is thermally activated. First one at low frequency corresponds to grain boundary and the second one at high frequency is due to the grain, based on the distribution of relaxation times. Also, it is observed that the centre of semicircles located below the abscissa (Z′) axis which suggests that the relaxation process in this material is of a non-Debye type [74].

Considering the excellent chemical, thermal stabilities and the existence of hydrogen-bonding networks in [Cu($C_{10}H_{24}N_4$)Br]Br, this compound can be potentially proton conducting materials along the H-bonding chain. The proton conductivity increases upon increasing the temperature due to higher mobility or diffusion of proton (or hydrogen atom) carriers i.e., proton transfers, or proton disordering [75-78].

Nyquist plots were analyzed using Zview Software [79]. All fitted curves at each temperature (313 K, 333 K, 353 K, 373 K and 393 K) show the good conformity of calculated lines with the experimental data (**Fig.12**). The best fits were obtained using an equivalent circuit realized by two cells in series, the first consist of a parallel combination of bulk resistance R_2 and fractal capacity CPE_2 and the second consist of a parallel combination of grain boundary resistance R_1 and fractal capacity CPE_1. These cells are attributed to the grain and grain boundaries effects. The calculated conductivity of the hybrid material increased from 1.49 10^{-4} S cm^{-1} at 293 K to 3.4610^{-4} S cm^{-1} at 313 K. At 393 K, the high conductivity is 1.47 10^{-2} S cm^{-1}. It is worth noting that, from 293 to 393 K, the conductivity of [Cu($C_{10}H_{24}N_4$)Br]Br increased by 2 orders of magnitude, indicating that the transport of load carrier in this hybrid is a thermally activated process, which is common for semiconductor material.

The fitted parameter obtained by the equivalent circuit used to calculate the conductivity of grain at several temperatures. The grain conductivity σ_g is determined according to the following expression: $\sigma_g = \frac{e}{R_g \times S}$

Where *S* and *e* are the area and the thickness of the sample, respectively, and R_g is the resistance of the grain resistance. The dependence of $Ln(\sigma_g T)$ versus $\frac{1000}{T}$ is presented in **Fig.13**.

This variation shows that σ_g decreases with increasing temperature which indicates that the electric conduction in this material is a thermally activated process and fits well by the Arrhenius law:$\sigma_g = \sigma_0 \exp(-\frac{E_a}{k \times T})$

Where σ_0 is the pre-exponential factor, E_a is the activation energy, *k* is the Boltzmann constant. Two regions were identified with changing of slope at T = 343±5 K which confirms the transition temperature observed in the thermal study (DSC). The calculated activation energies from linear fits to the data point are EaI = 0.30 eV in region I and EaII = 0.69 eV in region II. Hence, we assume that when the temperature was lower than 343 K, the combination of Grotthuss (hopping) mechanism (<0.4 eV) dominated the proton conduction, while at temperatures above 343, the vehicle mechanism (> 0.4 eV) guides the proton conduction [76,80].

4. Conclusion

The organic-inorganic Cu(II) bromide complex $[Cu(C_{10}H_{24}N_4)Br]Br$ has been synthesized, crystallized and characterized. It showed a phase transition at 343 K confirmed by the DSC measurements together with electric anomalies. The compound crystallizes in the orthorhombic system, with chiral space group $P2_12_12_1$ which exhibits the enantiomorphic crystal class 222 (D_2). Due to the presence of intrinsic hydrogen-bonding donors and acceptors, the compound exhibits a (3D) hydrogen-bonding interaction topology which is possibly an important aspect for proton conduction. Hirshfeld surface analyses revealed the effective role of H…Br and H…H contacts in the crystal packing. The optical properties at the absorption edge of copper (II) complex showed two distinct peaks at 261 and 565 nm, respectively. The values of the band gap energies direct and indirect are 3.91 and 3.5 eV, respectively, prove that the investigated compound is a semiconductor. The equivalent circuit was determined and the impedance spectra have revealed the contributions of grain and grain boundary in the proton conduction for this material.

Declaration of competing interest

The data that support the findings of this study are available from the corresponding author upon reasonable request. Additional supporting information may be found online in the Supporting Information section at the end of this article.

CRediT authorship contribution statement

Wassim MAALEJ: Conceptualization, Data curation, Formal analysis, Investigation, Methodology, Software, Validation, Writing – original draft, Writing – review & editing. **Philippe GUIONNEAU:** Investigation, Supervision, Validation, Writing – review & editing. **Zakaria ELAOUD:** Software, Validation, Writing – review & editing

Acknowledgements

The authors thank the University of Sfax-Tunisia for financial support. The X-ray diffraction is performed at the XRD center of ICMCB.

References

[1] S. Srivastava, R. Gupta, Metalloligands to material: Design strategies and network topologies, *CrystEngComm*, **2016**,18, 9185-9208.
https://doi.org/10.1039/C6CE01869F

[2] Y. Peng, L. Li, C. Zhu, B. Chen, M. Zhao, Z. Zhang, Z. Lai, X. Zhang, C. Tan, Y. Han, Y. Zhu, and H. Zhang, Intramolecular Hydrogen Bonding-Based Topology Regulation of Two-Dimensional Covalent Organic Frameworks, *J. Am. Chem. Soc*., **2020**, 142, 30, 13162–13169.
https://doi.org/10.1021/jacs.0c05596

[3] L. Li, F. Lu, H. Guo and W. Yang, A new two-dimensional covalent organic framework with intralayer hydrogen bonding as supercapacitor electrode materials, *Micropor. Mesopor. Mat*., **2021**, 312, 110766.
https://doi.org/10.1016/j.micromeso.2020.110766

[4] B.Morzyk-Ociepa, E. Rózycka-Sokołowska, D. Michalska, Revised crystal and molecular structure, FT-IR spectra and DFT studies of chlorotetrakis(imidazole)copper(II) chloride, *J. Mol Struct*.,**2012**, 1028, 49-56.
http://dx.doi.org/10.1016/j.molstruc.2012.06.028

[5] H. Yilmaz, S. Gorduk, O. Andac, Polymeric Ni(II) and Cu(II) complexes based on squaric acid and 1-vinylimidazole: Structural studies and hydrogen adsorption properties, *Inorg. Chim. Acta*, **2018**, 469,154-163.
http://dx.doi.org/10.1016/j.ica.2017.09.026

[6] Q. Wu, X. Liu, Y. Du, C. Teng, F. Liang, Nonlinear organic–inorganic halide hybrids containing unprecedented linear $[MIX_2]^-$ coordination units and quasi-two-dimensional lone pairs, *Chem. Commun.*, **2020**, 56, 4894-4897.
https://doi.org/10.1039/D0CC01532F

[7] X. Liu, Y. Wan, Q. Wu, F. Liang, J. Zhang, Structural Evolution and Optical Property Tunability by Halogen Substitution in $[N(CH_3)_4]MX_2$ ($M = Ga^+, In^+$, X = Cl, Br): A Family of Organically Templated Metal Halides, *Inorg. Chem.*, **2020**, 59, 10736–10745. https://doi.org/10.1021/acs.inorgchem.0c01189

[8] S. Zhao, X. Song, M. Zhu, X. Meng, L. Wu, S. Song, C. Wang, H. Zhang, Assembly of Three Coordination Polymers Based on a Sulfoniccarboxylic Ligand Showing High Proton Conductivity, *Dalton Trans*., **2015**,44, 948-954.
https://doi.org/10.1039/C4DT02870H

[9] R. Jaballi, W. Maalej, D. Atoui, H. Feki, R. Ben Salem, Z. Elaoud, Crystal packing, vibrational studies, DFT calculations of a new hybrid nickel (II)-complex and its application in Heck and Sonogashira cross- coupling reactions, *Appl. Organomet. Chem.*, **2018**, e4366.
https://doi.org/10.1002/aoc.4366
[10] H.Chowdhury, A. Bieńko, C. Rizzoli, C. Adhikary, Syntheses, structures and magnetic behaviors of 1D and 3D μ1,5-dicyanamide bridged copper(II) coordination polymers containing a symmetrical 1,2-dia- mine as a chelator, *Polyhedron*, **2020**, 188,114693.
https://doi.org/10.1016/j.poly.2020.114693
[11] K. Sultana, S. Zaib, N.ul Hassan Khan, I. Khan, K. Shahid, J. Simpson, J. Iqbal, Exploiting the potential of aryl acetamide derived Zn(II) complexes in medicinal chemistry: synthesis, structural analysis, assessment of biological profile and molecular docking studies, *New J.Chem.*, **2016**,40, 7084
https://doi.org/10.1039/C5NJ03531G
[12] T. Akutagawa, H. Koshinaka, D. Sato, S. Takeda, S. Noro, H. Takahashi, R. Kumai, Y. Tokura, T. Nakamura, Ferroelectricity and polarity control in solid-state flip-flop supramolecular rotators, *Nat. Mater*, **2009**, 8, 342-347.
https://doi.org/10.1038/nmat2377
[13] P. Guionneau, M. Marchivie, G. Chastanet, Multiscale approach of spin crossover materials - a concept mixing Russian dolls and domino effects, *Chem. Eur. J.*, **2021**, 27, 1483-1486.
https://doi.org/10.1002/chem.202002699
[14] N. N. Adarsh, M. M. Dîrtu, P. Guionneau, E. Devlin, Y. Sanakis, J. A. K. Howard, B. Chattopadhyay, Y. Garcia, One-Dimensional Looped Chain and Two-Dimensional Square Grid Coordination Polymers: Encapsulation of Bis(1,2,4-Triazole)-trans-cyclohexane into the Voids, *Eur. J. Inorg. Chem.*, **2019**, 585-591.
https://doi.org/10.1002/ejic.201801138
[15] A. M. Spokoyny, D. Kim, A. Sumrein, C. A. Mirkin, Infinite coordination polymer nano- and microparticle structures, *Chem. Soc. Rev.*, **2009**, 38, 1218-1227.
https://doi.org/10.1039/B807085G
[16] Y. Liao, S. K. Yang, K. Koh, A. J. Matzger, J. S. Biteen, Heterogeneous Single-Molecule Diffusion in One-, Two-, and Three-Dimensional Microporous Coordination Polymers: Directional, Trapped, and Immobile Guests, *Nano Lett.*, **2012**, 12, 3080-3085.
https://doi.org/10.1021/nl300971t

[17] S. Xiang, Y. He, Z. Zhang, H. Wu, W. Zhou, R. Krishna, B. Chen, microporous metal organic framework with potential for carbon dioxide capture at ambient conditions, *Nat. Commun.*, **2012**, 3, 1956-1959.
https://doi.org/10.1038/ncomms1956
[18] I. Ahmed, S. H.Jhung, Applications of metal-organic frameworks in adsorption/separation processes via hydrogen bonding interactions, *Chem. Eng. J.*, **2017**, 310, 197-215.
http://dx.doi.org/10.1016/j.cej.2016.10.115
[19] F. Hajlaoui, N. Audebrand, T. Roisnel, N. Zouari, Structural phase transition, electrical and semiconducting properties in a lead-free 2D hybrid perovskite-like compound: $[Cl\text{-}(CH_2)_2\text{-}NH_3]_2[CuCl_4]$, *Appl. Organomet. Chem*., **2019**, e5293.
https://doi.org/10.1002/aoc.5293
[20] L. Esmaeili, M. G. Perez, M.Jafari, J. Paquin, P. Ispas-Szabo, V. Pop, Marius Andruh, Joshua Byers, M. A.Mateescu, Copper complexes for biomedical applications: Structural insights, antioxidant activity and neuron compatibility, *J. Inorg. Biochem*., **2019**, 192, 87–97.
https://doi.org/10.1016/j.jinorgbio.2018.12.010
[21] E. P. Magennis , F. Fernandez-Trillo, C. Sui, S. G. Spain, D. J. Bradshaw, D. Churchley, G.Mantovani, K. Winzer, C. Alexander, Bacteria-instructed synthesis of polymers for self selective microbial binding and labelling, *Nat. Mater*, **2014**, 13, 748-755.
https://doi.org/10.1038/nmat3949
[22] H. Kwon, E. Lee, Coordination preference of hexa(2-pyridyl)benzene with copper(II) directed by hydrogen bonding, *CrystEngComm*, **2018**,20, 5233-5240.
https://doi.org/10.1039/C8CE00918J
[23] H. Eshtiagh-Hosseini, M. Mirzaei, M. Biabani, V. Lippolis, M. Chahkandi, C. Bazzicalupi, Insight into the connecting roles of interaction synthons and water clusters within different transition metal coordination compounds of pyridine-2,5-dicarboxylic acid: experimental and theoretical studies, *CrystEngComm*, **2013**, 15, 6752-6768.
https://doi.org/10.1039/C3CE40743H
[24] H. Yang, Z. Liang, B. Hao, X. Meng, Syntheses, crystal structures, and characterization of three 1D, 2D and 3D complexes based on mixed multidentate N- and O-donor ligands, *J. Solid StateChem.*, **2014**, 218, 23-31.
http://dx.doi.org/10.1016/j.jssc.2014.06.003
[25] J. Tao, R.-J. Wei, R.-B. Huang, L.-S. Zheng, Polymorphism in spin-crossover systems, *Chem. Soc. Rev.*, **2012**, 41, 703-737.
https://doi.org/10.1039/C1CS15136C

[26] Z. Xie, M. Feng, J. Li, X. Huang, Ionothermal synthesis and crystal structure of a 2D metal organic framework: $[emim]_2[Cd_2(btec)Br^2]$ (emim = 1-ethyl-3-methylimidazolium, btec = 1,2,4,5-benzenetetracarboxylate), *Inorg. Chem. Commun.*, **2008**, 11, 43-1146.
https://doi.org/10.1016/j.inoche.2008.06.023
[27] K. A. Kounavi, A. A. Kitos, E .E. Moushi, M. J. Manos, C. Papatriantafyllopoulou, A. J. Tasiopoulos, S. P. Perlepesa, V.Nastopoulos, Supramolecular features in the engineering of 3d metal complexes with phenyl-substituted imidazoles as ligands: the case of copper(II), *CrystEngComm*, **2015**, 17, 7510-7521.
https://doi.org/10.1039/c5ce01222h
[28] X. Ding, S. Wang, Y. Li, W. Huang, Inorganic anion-assisted supramolecular assemblies of bent dipyridines: effects of anionic geometries on the hydrogen-bonding networks, *Inorg. Chem. Front.*, **2015**, 2, 263-272.
https://doi.org/10.1039/C4QI00125G
[29] H. Zhao, X. Kong, H. Li, Y. Jin, L. Long, X. C. Zeng, R. Huang, L. Zheng, Transition from one-dimensional water to ferroelectric ice within a supramolecular architecture, *PNAS*, **2011**, 108, 3481-3486.
https://doi.org/10.1073/pnas.1010310108
[30] M. G. Reeves, E. Tailleur, P. A. Wood, M. Marchivie, G. Chastanet, P. Guionneau, S. Parsons, Mapping the cooperativity pathways in spin crossover complexes, *Chem. Sci.*, **2021**, 12, 1007-1015.
https://doi.org/10.1039/D0SC05819J
[31] X. Liang, T. Cao, L. Wang, C. Zheng, Y. Zhao, F. Zhang, C. Wen, L. Feng, C. Wan, From organic ligand to metal-organic coordination polymer, and to metal-organic coordination polymer-cocrystal composite: a continuous promotion of proton conductivity of crystalline materials, *CrystEngComm*, **2020**, 22, 1414-1424.
https://doi.org/10.1039/C9CE01716J
[32] H. Zhu, Y. Wu, G. Zhang, Y. Lou, J. Hu, Side-chain-modulated supramolecular assembly between CuX_2 (X = Cl, Br) and quasi-planar p-conjugated organic synthons of 1, 3, 5-tris(2-alkylthiolpyrimidinyl)benzene: Crystal structures and conductive properties, *Polyhedron*, **2015**, 85,60-68.
http://dx.doi.org/10.1016/j.poly.2014.08.051

[33] M. Wei, J.Fu, Y. Wang, J. Gu, B. Liu, H. Zang, E. Zhou, K. Shao, Z. Su, Changes of coordination modes of Cu-based coordination complexes as tuneable proton-conducting solid electrolytes, *J. Mater. Chem. A*, **2017**, 5, 1085-1093.
https://doi.org/10.1039/C6TA08581D
[34] A. Garai, A. G. Kumar, S. Banerjee, K. Biradha, Proton Conducting Hydrogen-Bonded 3D-Frameworks of Imidazo-Pyridine-Based Coordination Complexes Containing Naphthalene Disulfonates in Rhomboid Channels,*Chem. Asian J.*, **2019**, 14, 4389-4394.
https://doi.org/10.1002/asia.201901338
[35] H. Ye, D. Fu, Y. Zhang, W. Zhang, R. Xiong, S. D. Huang, Hydrogen-Bonded Ferroelectrics Based on Metal-Organic Coordination,*J. Am. Chem. Soc.*, **2009**, 131, 1, 42-43.
https://doi.org/10.1021/ja808331g
[36] M. Wei, J. Fu, Y. Wang, J. Gu, B. Liu, H. Zang, E. Zhou, K. Shao, Z. Su, High tuneable proton-conducting coordination polymers derived from sulfonate-based ligand, *J. Mater. Chem. A*, **2017**, 19, 7050-7056.
https://doi.org/10.1039/C7CE01589E
[37] M. Viswanathan, Disorder in the hydrogen-atoms uninvolved in hydrogen bonds in a metal–organic framework, *Phys.Chem. Chem. Phys.*, **2018**,20, 24527-24534.
https://doi.org/10.1039/C8CP03709D
[38] C. Chen, F. Wang, Y. Zhang, Q. Ye, H. Ye, D. Fu, A high-temperature supramolecular-based switchable dielectric material with electrical bistability between high and low dielectric states, *CrystEngComm.*, **2015**,17, 2479-2485.
https://doi.org/10.1039/C4CE02028F
[39] M.Moskwa, G. Bator, M. Rok, W. Medycki, A. Miniewicz, R. Jakubas, Investigations of organic-inorganic hybrids based on homopiperidinium cation with haloantimonates(III) and halobismuthates(III). Crystal structures, reversible phase transions, semiconducting and molecular dynamic properties., *Dalton Trans*., **2018**, 47, 13507-13522.
https://doi.org/10.1039/C8DT03121E
[40] H. D. Duncan, M. T. Dove, D. A. Keenb, A. E. Phillips, Local structure of the metal–organic perovskite dimethylammonium manganese(II) format, *Dalton Trans.*, **2016**, 45, 4380-4391.
https://doi.org/10.1039/C5DT03687A
[41] APEX2 program suite V2014.11–0, Bruker AXS Inc., Wisconsin, USA.
[42] G.M. Sheldrick, SAINT Version 8.37A, Bruker AXS Inc., Wisconsin, USA, 2013.

[43] G. M. Sheldrick, SADABS version 2014/5, SADABS Bruker AXS Inc., Madison, Wisconsin, USA.

[44] G. Sheldrick, SHELXT-Integrated space-group and crystal-structure determination, *Acta Cryst. A*, **2015**, A71, 3-8.
https://doi.org/10.1107/S2053273314026370

[45] G. Sheldrick, Crystal structure refinement with SHELXL, *Acta Cryst.C*, **2015**, C71, 3-8.
https://doi.org/10.1107/S2053229614024218

[46] L. J. Farrugia, WinGX and ORTEP for Windows: an update, *J. Appl. Crystallogr.*, **2012**, 45, 849-854.
doi.org/10.1107/S0021889812029111

[47] W. T. Pennington, DIAMOND – Visual Crystal Structure Information System, *J. Appl. Crystallogr*., **1999**, 32, 1028 -1029.
https://doi.org/10.1107/S0021889899011486

[48] Hirshfeld, F. L., Bonded-Atom Fragments for Describing Molecular Charge Densities, *Theoret. Chim. Acta*, **1977**, 44, 129-138.
https://doi.org/10.1007/BF00549096

[49] M. J. Turner, J. J. McKinnon, S. K. Wolff, D. J. Grimwood, P. R. Spackman, D. Jayatilaka, M.A. Spackman, *CrystalExplorer*, **2017**, The University of Western Australia.

[50] Y. Mei, X. Hua, J. Gao, W. Liao, Switchable dielectric phase transition behaviors in two organicinorganic copper(II) halides with distinct coordination geometries, *CrystEngComm*, **2018**, 20, 6261-6266.
https://doi.org/10.1039/C8CE01263F

[51] A. Sen, S. Roy, S. C. Peter, A. Paul, U. V. Waghmare, S. Athinarayanan, Order-Disorder Structural Phase Transition and Magnetocaloric Effect in Organic-Inorganic Halide Hybrid $(C_2H_5NH_3)_2CoCl_4$, *J. Solid StateChem.*, **2018**, 258,431-440.
https://doi.org/10.1016/j.jssc.2017.10.036

[52] A. W. Addison, T. N. Rao, J. Reedijk, J. van Rijn, G. C. Verschoor, Synthesis, structure, and spectroscopic properties of copper(II) compounds containing nitrogen–sulphur donor ligands; the crystal and molecular structure of aqua[1,7-bis(N-methylbenzimidazol-2′-yl)-2,6-dithiaheptane]copper(II) perchlorate, *J. Chem. Soc., Dalton Trans.*, **1984**, 1349-1356. https://doi.org/10.1039/DT9840001349.

[53] I. Warad, S. Musameh, A. Sawafta, P. Brandão, C. J. Tavares, A. Zarrouk, S. Amereih, A. A. Ali, R. Shariah, Ultrasonic synthesis of Oct. *trans*-$Br_2Cu(N \cap N)_2$ Jahn-Teller distortion

complex: XRD-properties, solvatochromism, thermal, kinetic and DNA binding evaluations, *Ultrason. Sonochem.*, **2019**, 52,428–436.
https://doi.org/10.1016/j.ultsonch.2018.12.019
[54] J. Conradie, M. M. Conradie, K. M. Tawfiq, S. J. Coles, G. J. Tizzard, C. Wilson, J. H. Potgieter, Jahn-Teller distortion in 2-pyridyl-(1,2,3)-triazole-containing copper(II) compounds, *New J. Chem.*, **2018**, 42, 16335-16345.
https://doi.org/10.1039/C8NJ03080D
[55] S. S. Massoud, F. A. Mautner, Synthesis, characterization, and crystal structure of 1,4 bis(3-aminopropyl)piperazineperchloratocopper(II) perchlorate, *Inorg.Chem. Commun.*, **2004**, 7, 559-562.
https://doi.org/10.1016/j.inoche.2004.02.013
[56] F. A. Saleemh, S. Musameh, A. Sawafta, P. Brandao, C. J. Tavares, S. Ferdov, A. Barakat, A. A. Ali, M. Al-Noaimi, I. Warad, Diethylenetriamine/diamines/copper (II) complexes [Cu(dien)(NN)]Br_2: Synthesis, solvatochromism, thermal, electrochemistry, single crystal, Hirshfeld surface analysis and antibacterial activity, *Arab. J. Chem.*, **2017**, 10, 845–854.
http://dx.doi.org/10.1016/j.arabjc.2016.10.008
[57] A. Kessentini, M. Belhouchet, J. J. Suñol, Y. Abid, T. Mhiri, Crystal structure, vibrational studies and optical properties of a new organic–inorganic hybrid compound $(C_{10}H_{28}N_4)CuCl_5Cl_4H_2O$, *Spectroc. Acta A*, **2015**, 134, 28-33.
http://dx.doi.org/10.1016/j.saa.2014.06.073
[58] Z. Smékal, T. Maris, M. Korabik, Structure and magnetic properties of binuclear [Cu(amppz)(μ- NC)Fe$(CN)_4$NO] (amppz = 1,4-bis(3- aminopropyl)piperazine), *J. Coord. Chem.***, 2014**, 67, 3167-3175.
http://dx.doi.org/10.1080/00958972.2014.962524
[59] S. S. Batsanov, Van der Waals Radii of Elements, *Inorg. Mater.*, **2001**, 37, 871-885.
https://doi.org/10.1023/A:1011625728803
[60] A. Khan, N. Ali, M. Bilal, S. Malik, S. Badshah, H. M. N. Iqbal, Engineering Functionalized Chitosan-Based Sorbent Material: Characterization and Sorption of Toxic Elements, *Appl. Sci.*, **2019**, 9, 5138.
https://doi.org/10.3390/app9235138
[61] S. Y. AlQaradawi, A. Mostafa, H. S. Bazzi, Synthesis, spectroscopic and thermal studies of charge-transfer molecular complexes formed in the reaction of 1,4-bis (3-aminopropyl) piperazine with σ- and π acceptors, *J. Mol. Struct.*, **2012**, 1011, 172-180.
https://doi.org/10.1016/j.molstruc.2012.01.002

[62] T. Moumene, E. H. Belarbi, B. Haddad, D. Villemin, O. Abbas, B. Khelifa, S. Bresson, Vibrational Spectroscopic Study of Imidazolium Dicationic Ionic Liquids: Effect of Cation Alkyl Chain Length , *J. Appl. Spectrosc.*, **2016**, 83, 165-171.
https://doi.org/10.1007/s10812-016-0264-7
[63] A. W. Herlinger, S. L. Wenhold, T. V. Long, Infrared Spectra of Amino Acids and Their Metal Complexes. II. Geometrical Isomerism in Bis(amino acidato)copper(II) Complexes, *J. Am. Chem. Soc.*, **1970**, 92, 22, 6474-6481.
https://doi.org/10.1021/ja00725a015
[64] Y. Liu, Z. Zhao, Z. Fang, R. Yu, C. Lu, A 2D Cu(I) triazolate coordination polymer: Synthesis and characterization of $[Cu_4Br_4(C_8H_8N_4)_2]H_2O$, *Inorg. Chem. Commun.*, **2009**, 12, 599-601.
https://doi.org/10.1016/j.inoche.2009.04.030
[65] D. Cortecchia, H. A. Dewi, J. Yin, A. Bruno, S. Chen, T. Baikie, P. P. Boix, M. Graïtzel, S. Mhaisalkar, C. Soci, N. Mathews, Lead-Free $MA_2CuCl_xBr_{4-x}$ Hybrid Perovskites, *Inorg. Chem.*, **2016**, 55, 1044-1052.
https://doi.org/10.1021/acs.inorgchem.5b01896
[66] P. K. Olshin, O. S. Myasnikova, M. V. Kashina, A. O. Gorbunov, N.A. Bogachev, V.O. Kompanets, S. V. Chekalin, S. A. Pulkin, V. A. Kochemirovsky, M. Yu. Skripkin, A. S. Mereshchenko, The electronic spectra and the structures of the individual copper(II) chloride and bromide complexes in acetonitrile according to steady-state absorption spectroscopy and DFT/TD-DFT calculations, *Chem. Phys*., **2018**, 503, 14-19.
https://doi.org/10.1016/j.chemphys.2018.01.020
[67] M. Ulutagay-Kartin, S. Hwu, J. A. Clayhold, Nanostructured Magnetic Cuprate Cluster: Synthesis, Structure, UV−Vis Spectroscopy, and Magnetic Properties of a New Copper(II) Arsenate $NaCuAsO_4$ Containing Discrete $[Cu_4O_{16}]^{24-}$ Clusters, *Inorg. Chem.*, **2003**, 42, 7, 2405-2409.
https://doi.org/10.1021/ic026169q
[68] E. R. Dohner, E. T. Hoke, H. I. Karunadasa, Self-Assembly of Broadband White-Light Emitters, J. Am. Chem. Soc., **2014**, 136, 1718–1721.
https://doi.org/10.1021/ja411045r.
[69] T. Hu, M. D. Smith, E. R. Dohner, M.-J. Sher, X. Wu, M. T. Trinh, A. Fisher, J. Corbett, X.-Y. Zhu, H. I. Karunadasa, A. M. Lindenberg, Mechanism for Broadband White-Light Emission from Two-Dimensional (110) Hybrid Perovskites, J. Phys. Chem. Lett., **2016**, 7, 2258–2263.

https://doi.org/10.1021/acs.jpclett.6b00793.

[70] C. V. Ramana, G. Carbajal-Franco, R. S. Vemuri, I. Troitskaia, S. Gromilov, V.V. Atuchin, Optical properties and thermal stability of germanium oxide (GeO_2) nanocrystals with α-quartz structure. Mater. Sci. Eng. B, **2010**, 174, 279–284.
https://doi.org/10.1016/j.mseb.2010.03.060.

[71] P. D. Harvey, C. Reber, Distortions in square-planar palladium(II) halides: a nonempirical molecular orbital model study, *Can. J. Chem.*, **1999**, 77, 16-23.
https://doi.org/10.1139/v98-212

[72] A. H. Ammar, A. A. M. Farag, M. S. Abo-Ghazala, Influence of Sb addition on the structural and optical characteristics of thermally vacuum evaporated Sb_xSe_{1-x} thin films, *J. Alloy. Comp.*, **2017**, 694, 752-760.
https://doi.org/10.1016/j.jallcom.2016.10.042

[73] H. Li, Y. Liu, X. Chen, J. Gao, Z. Wang, W. Liao, High-Temperature Dielectric Switching and Photoluminescence in a Corrugated Lead Bromide Layer Hybrid Perovskite Semiconductor, *Inorg. Chem.*, **2019**, 58, 10357-10363.
https://doi.org/10.1021/acs.inorgchem.9b01538

[74] G. Williams, D. C. Watts, Non-Symmetrical Dielectric Relaxation Behaviour Arising from a Simple Empirical Decay Function, *Trans. Faraday Soc.*, **1970**, 66, 80-85.
https://doi.org/10.1039/TF9706600080

[75] A. Ueda, S. Yamada, T. Isono, H. Kamo, A. Nakao, R. Kumai, H. Nakao, Y. Murakami, K. Yamamoto, Y. Nishio, H. Mori, Hydrogen-Bond-Dynamics-Based Switching of Conductivity and Magnetism: A Phase Transition Caused by Deuterium and Electron Transfer in a Hydrogen-Bonded Purely Organic Conductor Crystal, *J. Am. Chem. Soc.*, **2014**, 136, 12184–12192.
https://doi.org/10.1021/ja507132m

[76] Y.Wei, X. Hu, Z. Han, X. Dong, S. Zang, T. C. W. Mak, Unique Proton Dynamics in an Efficient MOF-Based Proton Conductor, *J. Am. Chem. Soc.*, **2017**, 139, 9, 3505-3512.
https://doi.org/10.1021/jacs.6b12847

[77] A. Katrusiak, M. Szafranski, Disproportionation of Pyrazine in $NH^{+\cdots}N$ Hydrogen-Bonded Complexes: New Materials of Exceptional Dielectric Response, *J. Am. Chem. Soc.*, **2006**, 128, 15775-15785.
https://doi.org/10.1021/ja0650192

[78] M. Bazaga-García, G. K. Angeli, K. E. Papathanasiou, I. R. Salcedo, P. Olivera-Pastor, E. R. Losilla, D. Choquesillo-Lazarte, G. B. Hix, A.Cabeza, K. D. Demadis, Luminescent and

Proton Conducting Lanthanide Coordination Networks Based On a Zwitterionic Tripodal Triphosphonate, *Inorg. Chem.*, **2016**, 55, 7414–7424.
https://doi.org/10.1021/acs.inorgchem.6b00570
[79] D. Johnson, Zview version 3.1c, Scribner Associates, **1990**.
[80] Z. Xu, Y.-L. Wong, R. Xiao, Y.Hou, Electronic and Ionic Conductivity of Metal-Organic Frameworks, *Comprehensive Supramolecular Chemistry II*, **2017**, 7, 399-423.
http://dx.doi.org/10.1016/B978-0-12-409547-2.13783-7

Figure captions:

Fig.1 Reactional scheme giving [Cu($C_{10}H_{24}N_4$)Br]Br and photos of crystals.

Fig.2 DSC curves of [Cu($C_{10}H_{24}N_4$)Br]Br at 5 K min^{-1}.

Fig.3 The asymmetric unit for the title compound of general formula [Cu($C_{10}H_{24}N_4$)Br]Br.

Fig.4 View of the crystal packing showing the 1-D network of [Cu($C_{10}H_{24}N_4$)Br]Br along *b*-axis.

Fig.5 View of the crystal packing showing the 2-D network of [Cu($C_{10}H_{24}N_4$)Br]Br in the bc plane.

Fig.6 View of the crystal packing showing the 3-D structure of [Cu($C_{10}H_{24}N_4$)Br]Br along the [100].

Fig.7 Experimental IR spectrum of the [Cu($C_{10}H_{24}N_4$)Br]Br.

Fig. 8 a) Hirshfeld surfaces of the asymmetric unit [Cu($C_{10}H_{24}N_4$)Br]Br;
b) Fingerprint plots of [Cu($C_{10}H_{24}N_4$)Br]Br complex.

Fig. 9 UV–vis Absorption spectra of [Cu($C_{10}H_{24}N_4$)Br]Br.

Fig. 10 The Tauc plot deduced from the optical spectrum of [Cu($C_{10}H_{24}N_4$)Br]Br.

Fig. 11 Temperature dependence of Nyquist diagram for [Cu($C_{10}H_{24}N_4$)Br]Br.

Fig. 12 Equivalent circuits for [Cu($C_{10}H_{24}N_4$)Br]Br.

Fig. 13 Variation of the ln (σ_g) versus 1000/T for [Cu($C_{10}H_{24}N_4$)Br]Br showing the phase transition temperature.

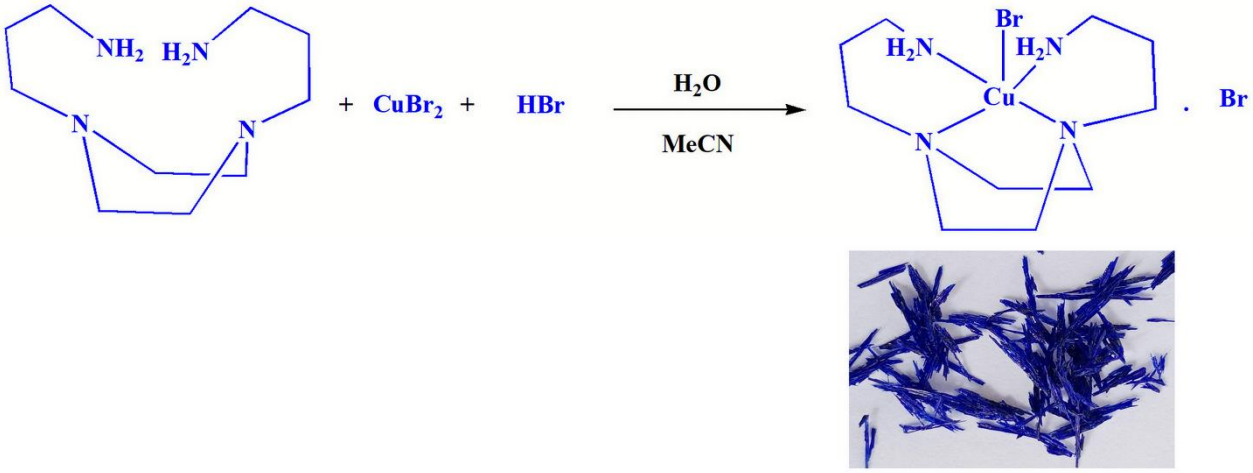

Fig.1

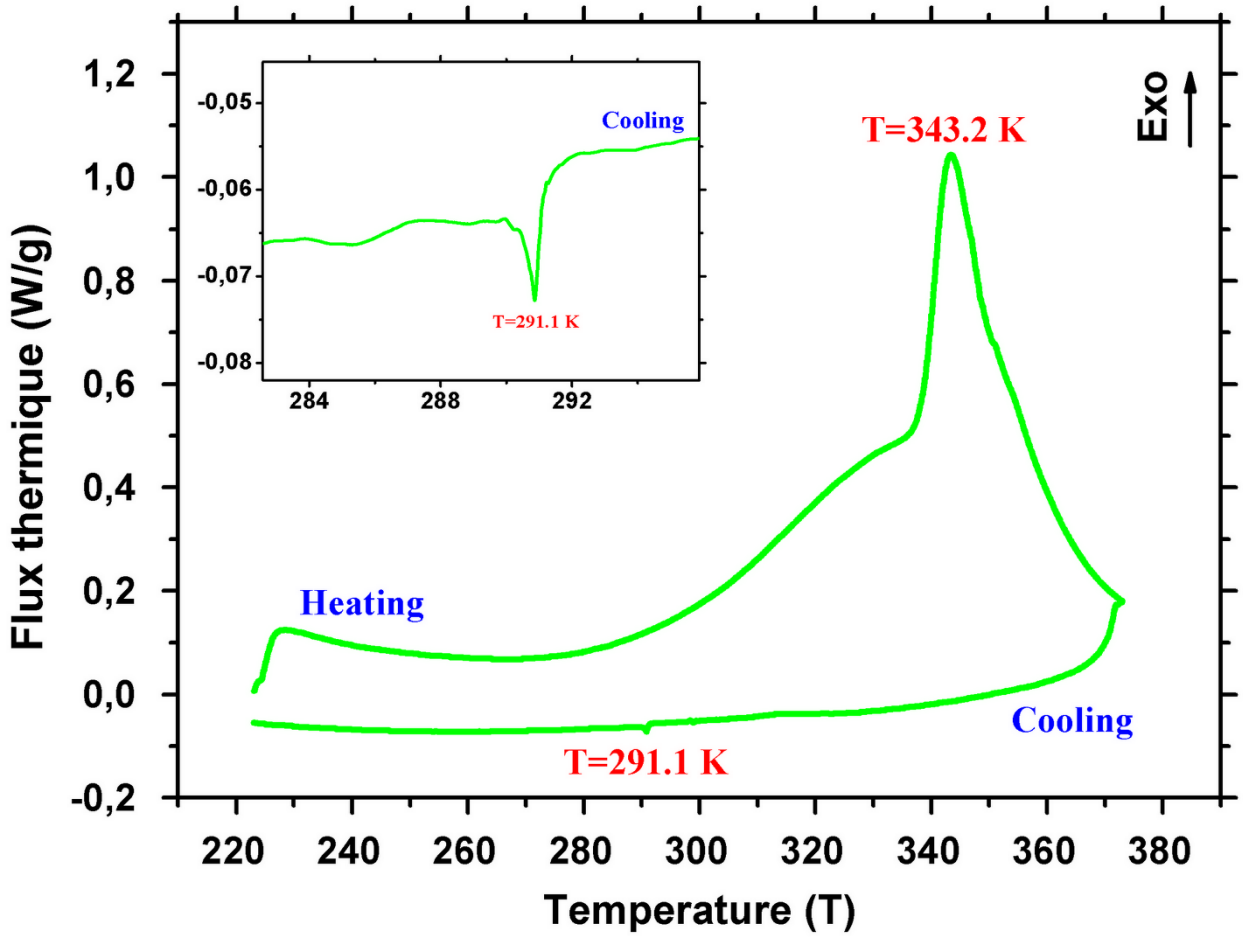
Flux thermique (W/g)
Temperature (T)
Exo
T=343.2 K
T=291.1 K
Heating
Cooling
Cooling
T=291.1 K
1,2
1,0
0,8
0,6
0,4
0,2
0,0
-0,2
220
240
260
280
300
320
340
360
380
-0,05
-0,06
-0,07
-0,08
284
288
292

Fig.2

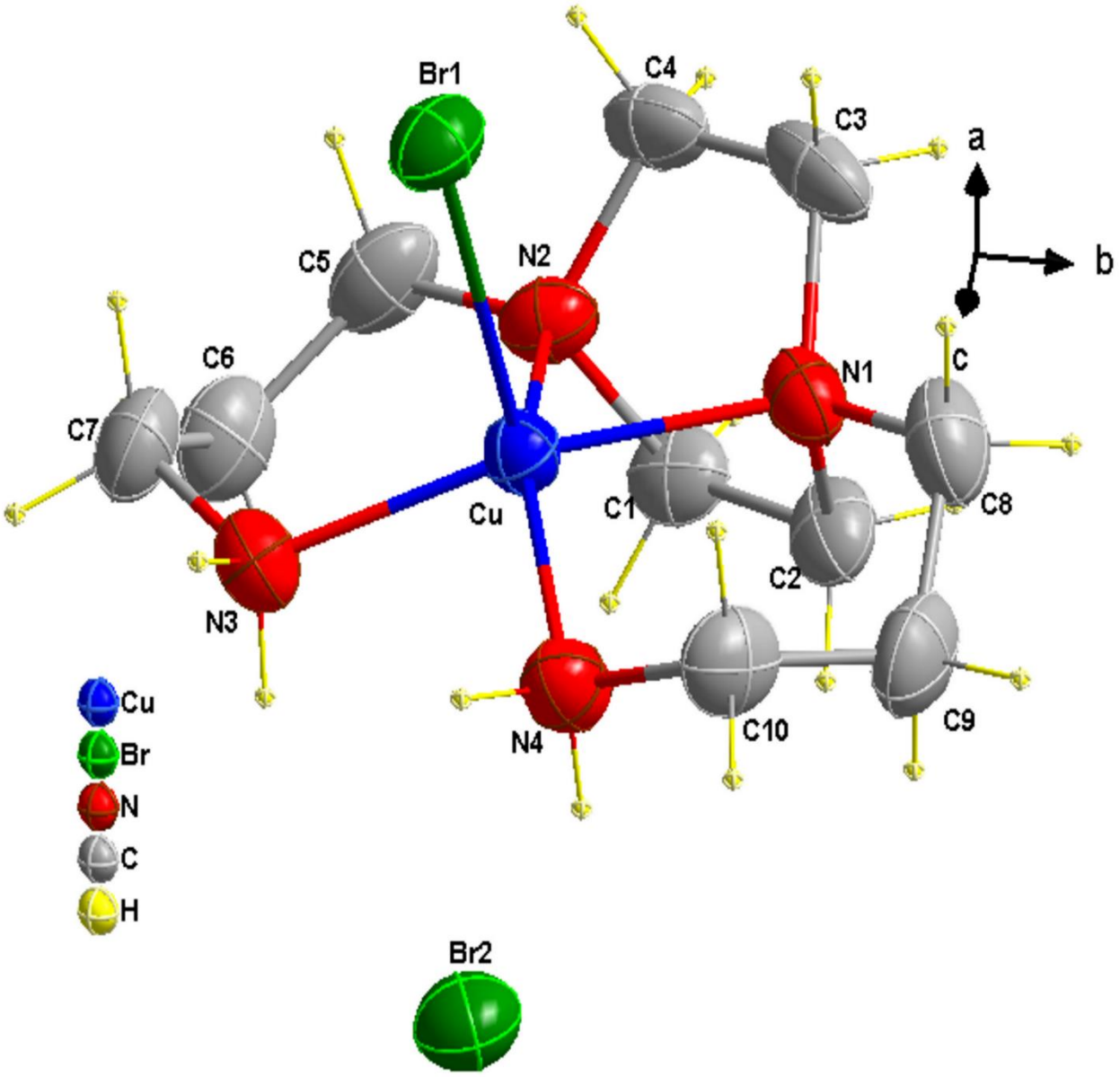

Fig.3

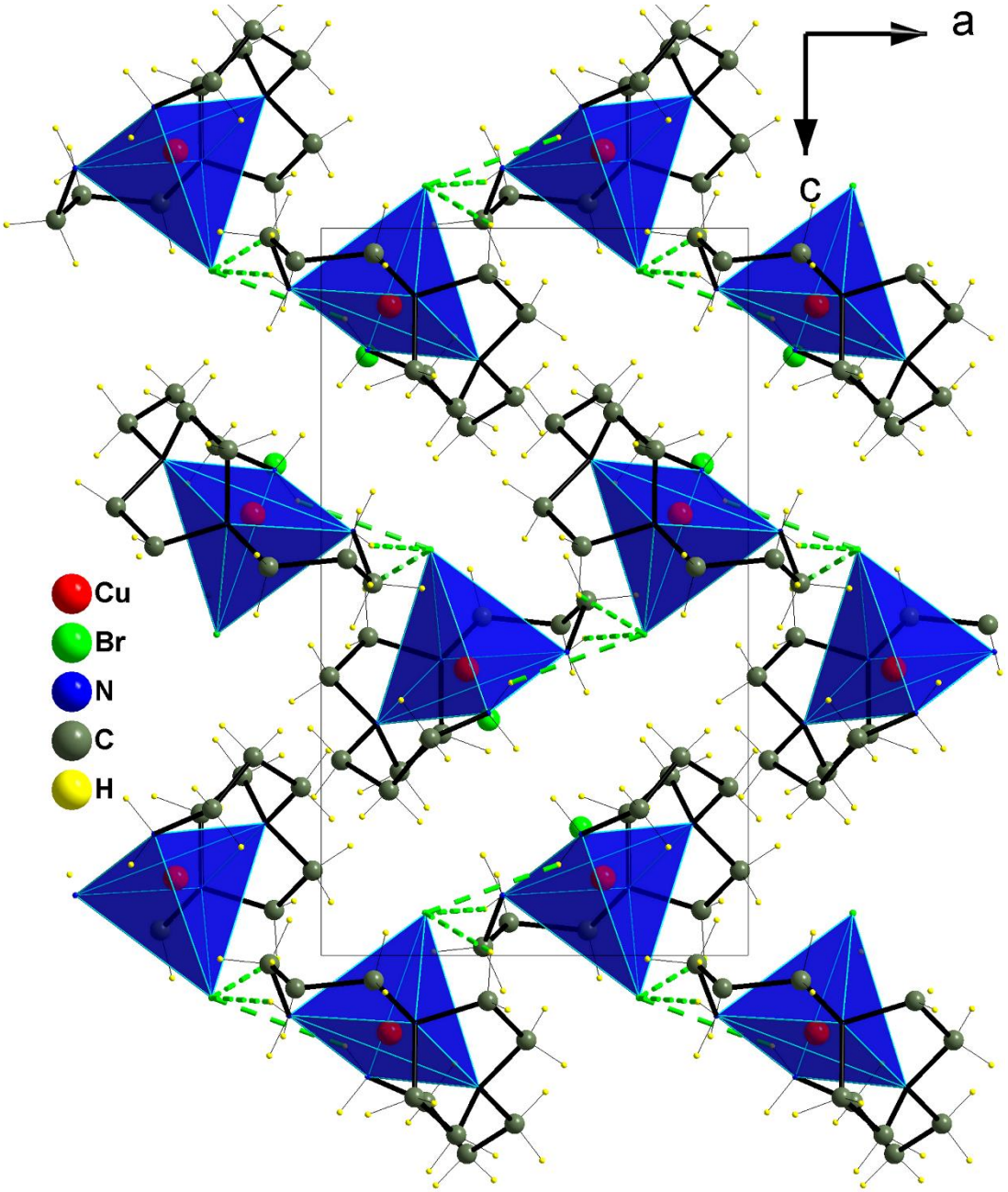

Fig.4

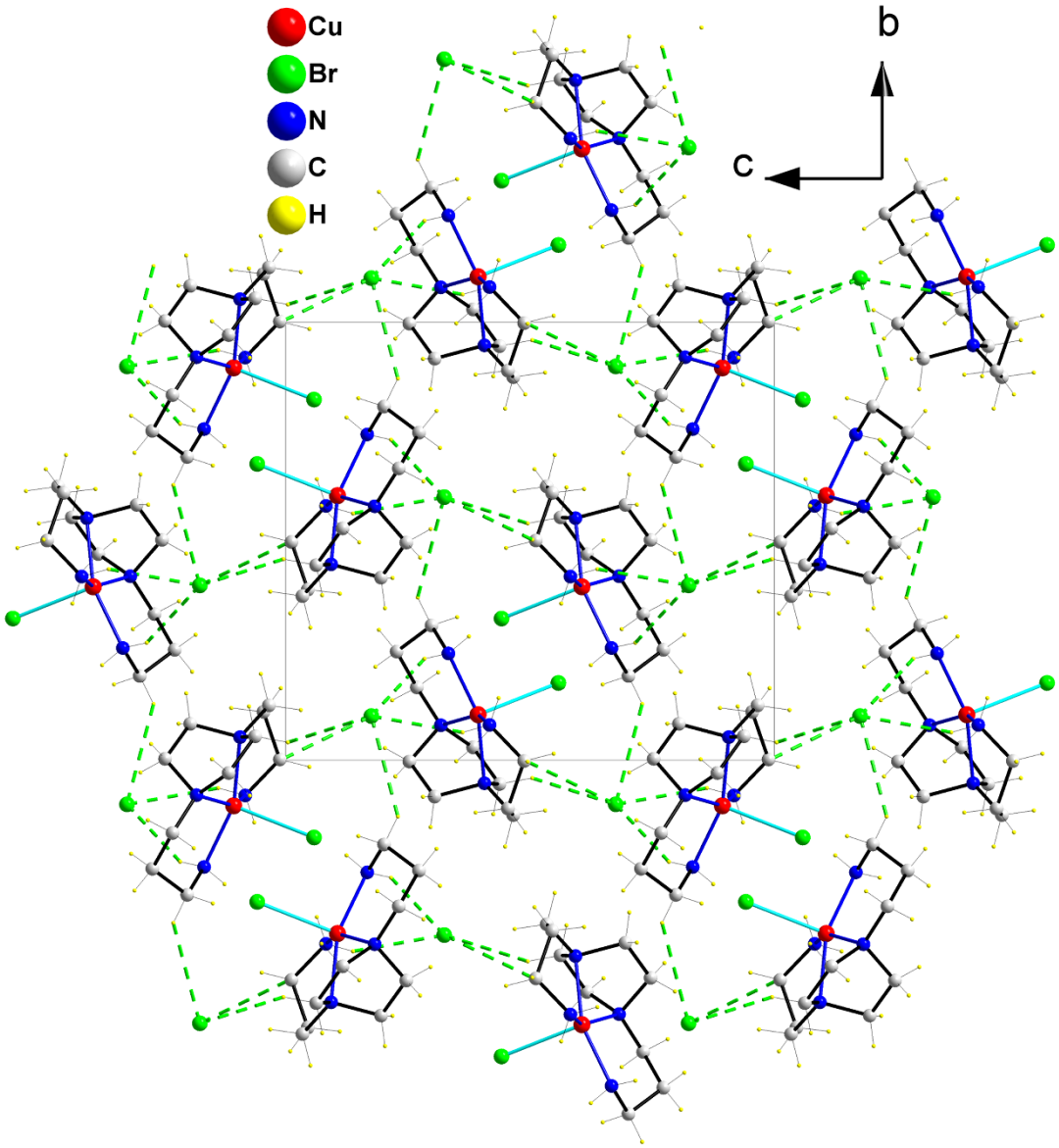

Fig.5

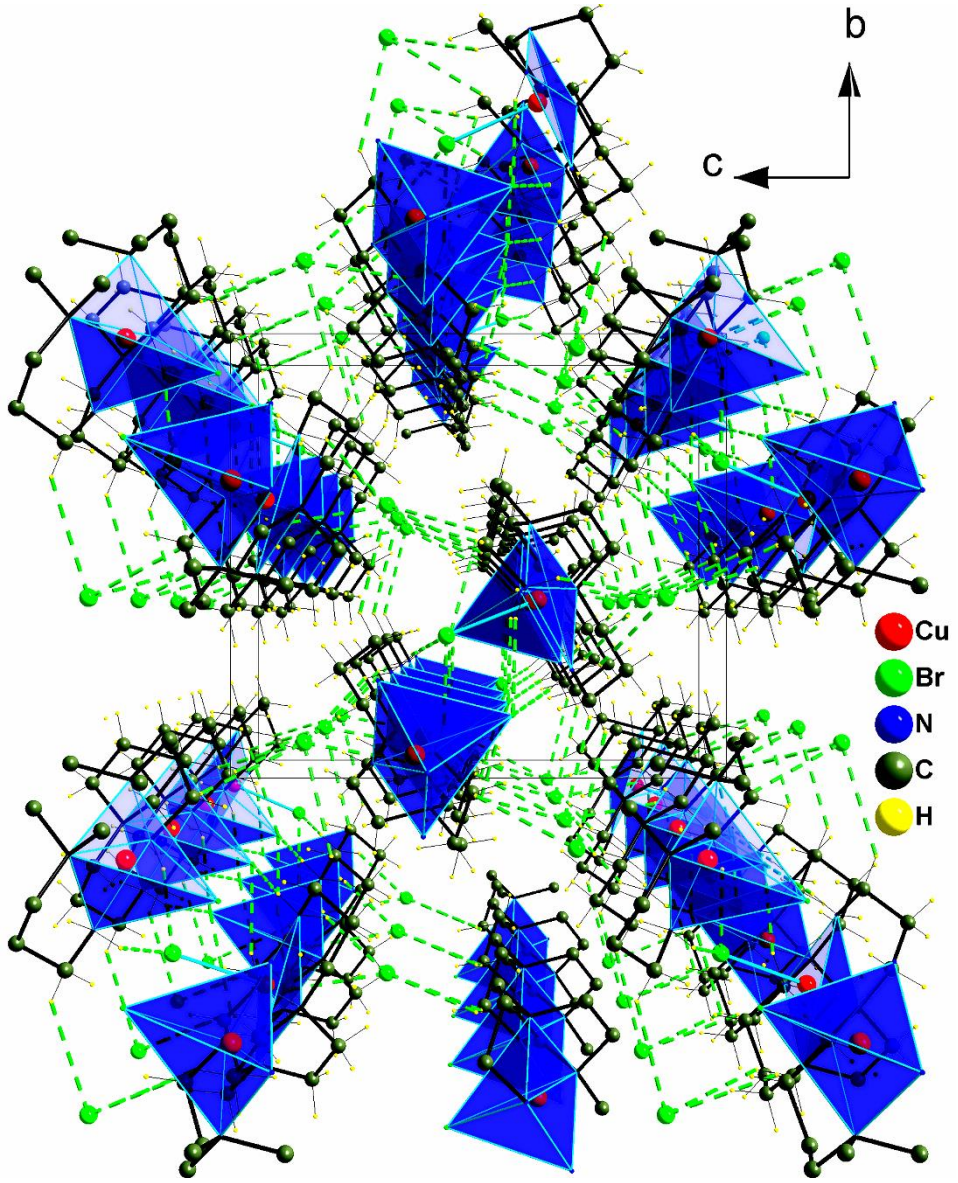

Fig.6

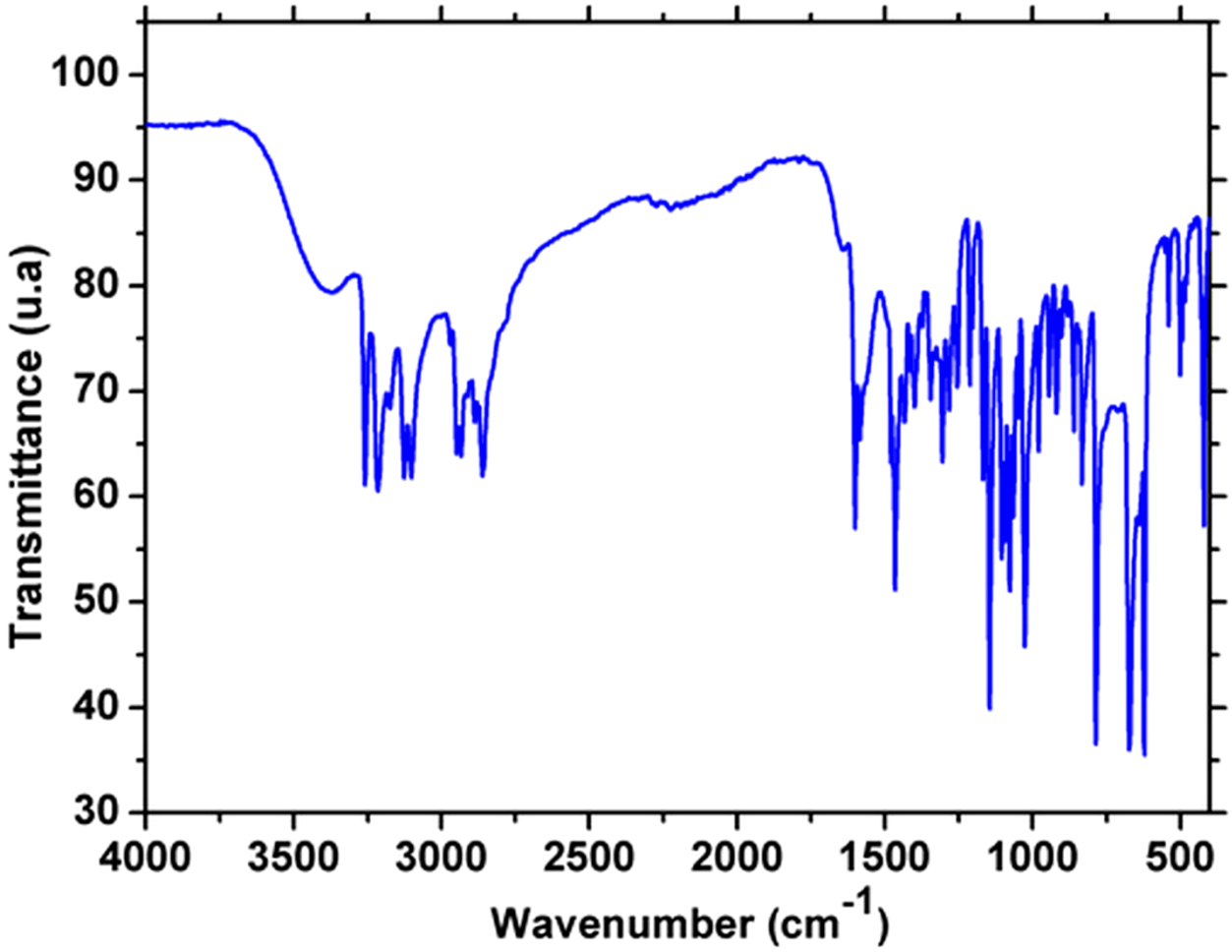
Transmittance (u.a)
100
90
80
70
60
50
40
30
4000
3500
3000
2500
2000
1500
1000
500
Wavenumber (cm-1)

Fig.7

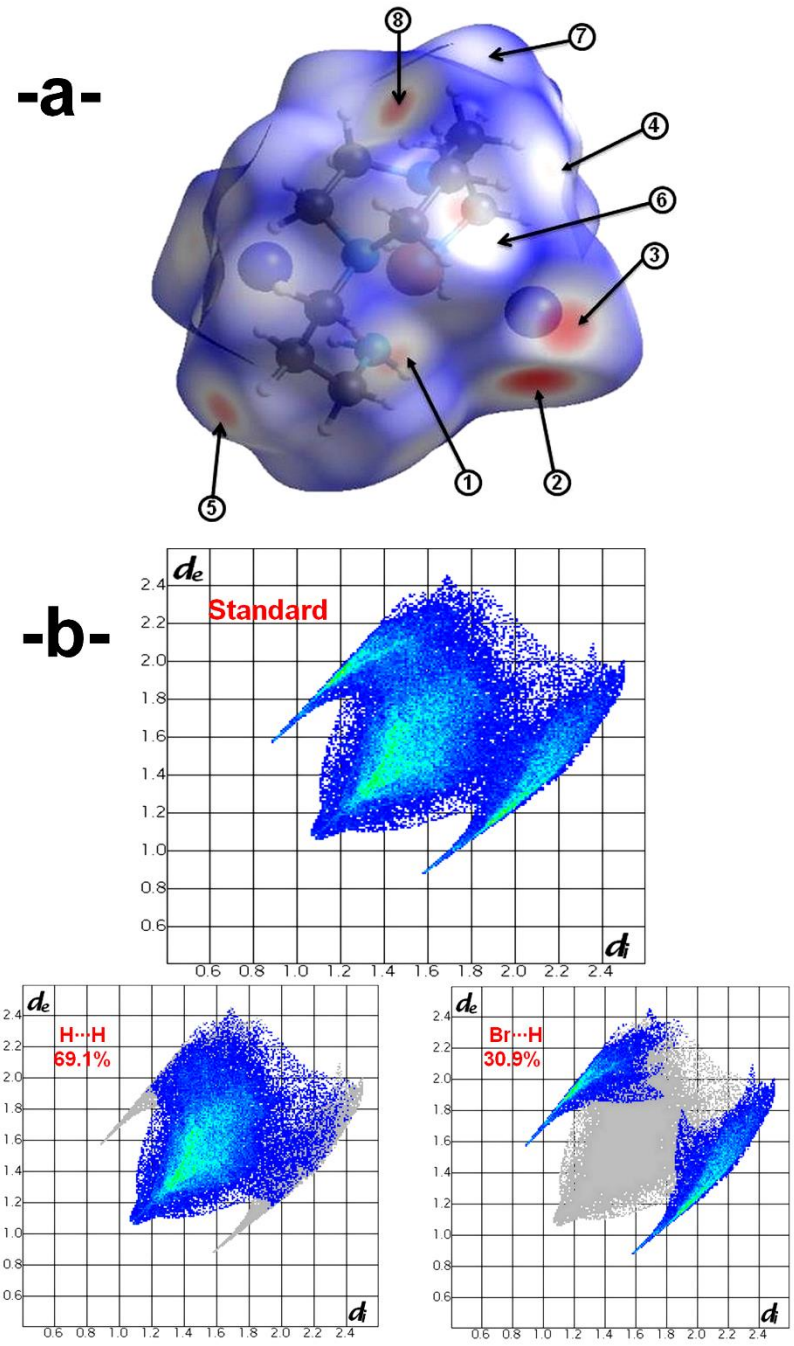
-a-
8
7
4
6
3
1
2
5
-b-
de
Standard
di
H···H
69.1%
Br···H
30.9%
0.6 0.8 1.0 1.2 1.4 1.6 1.8 2.0 2.2 2.4

Fig.8a

Fig.8b

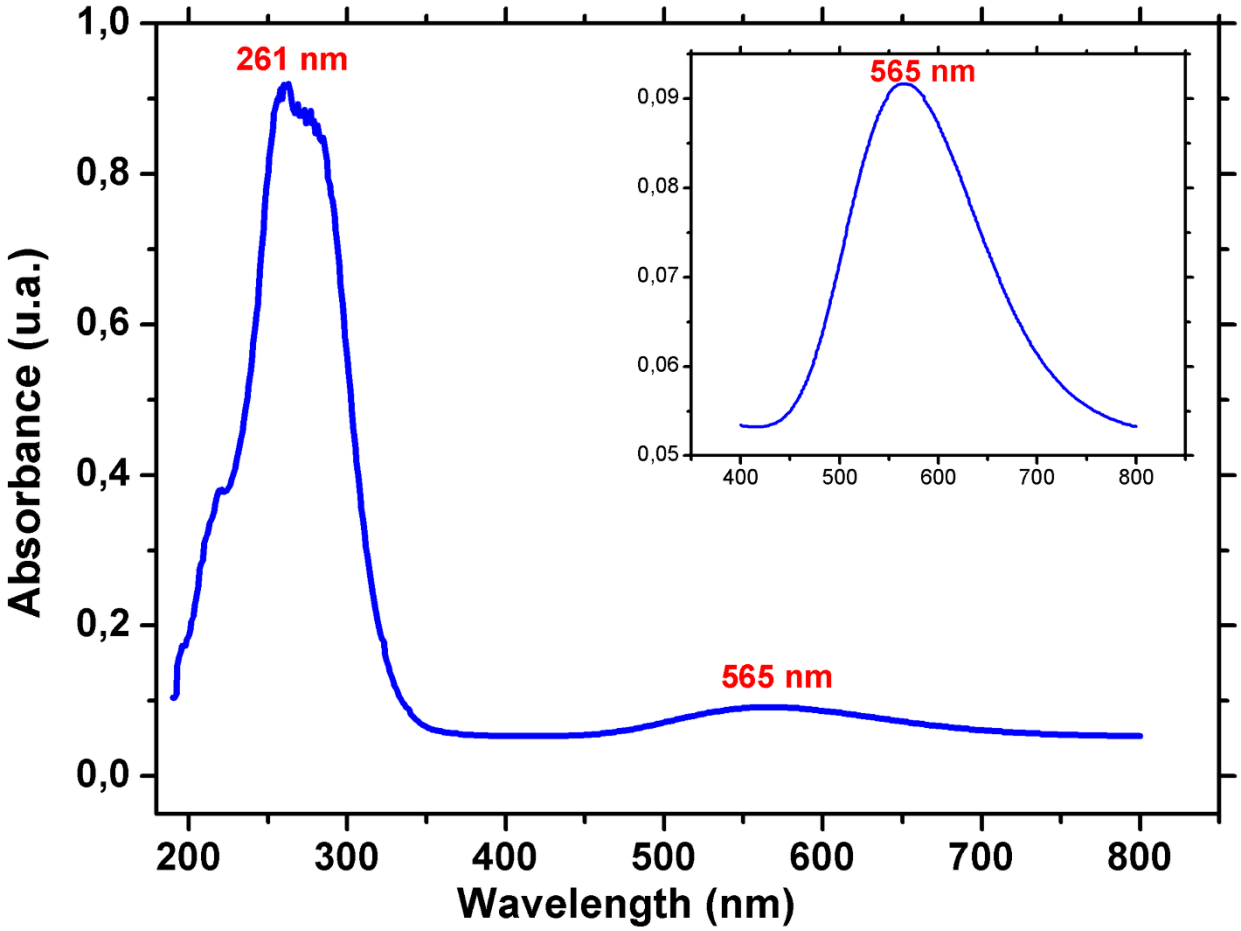
261 nm
565 nm
565 nm
Absorbance (u.a.)
Wavelength (nm)
1,0
0,8
0,6
0,4
0,2
0,0
200
300
400
500
600
700
800
0,09
0,08
0,07
0,06
0,05
400
500
600
700
800

Fig.9

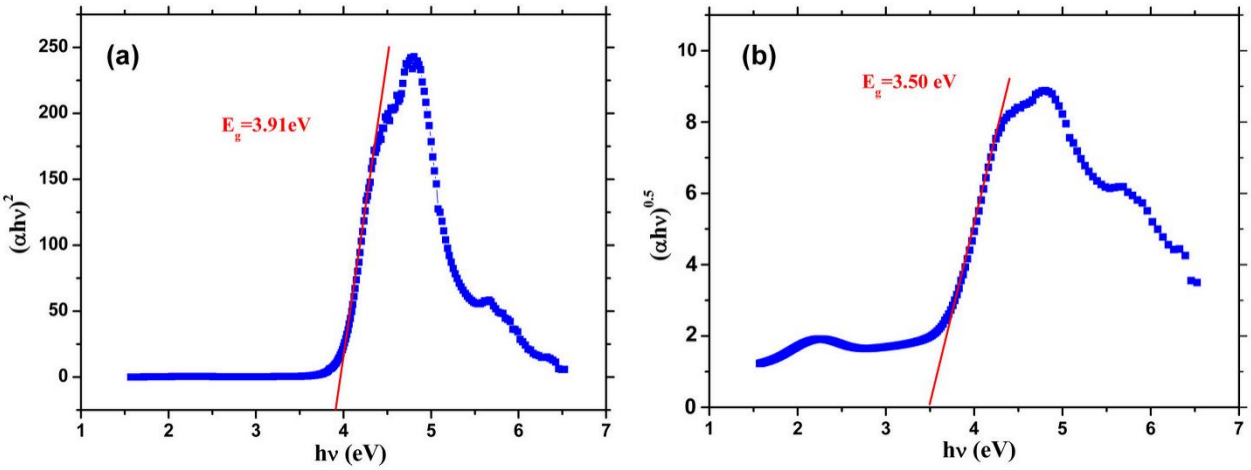

Fig.10

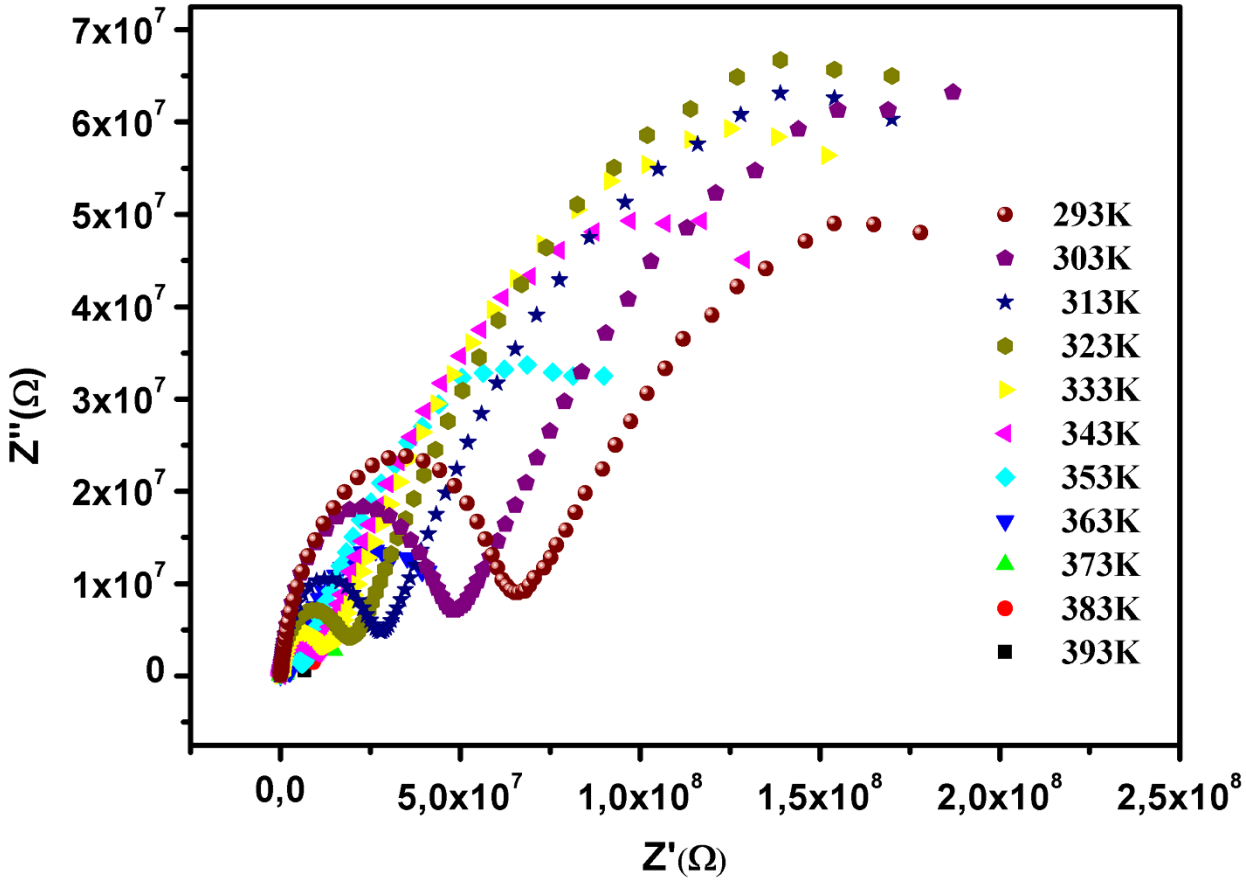
7x10^7
6x10^7
5x10^7
4x10^7
3x10^7
2x10^7
1x10^7
0
Z''(Ω)
0,0
5,0x10^7
1,0x10^8
1,5x10^8
2,0x10^8
2,5x10^8
Z'(Ω)
293K
303K
313K
323K
333K
343K
353K
363K
373K
383K
393K

Fig.11

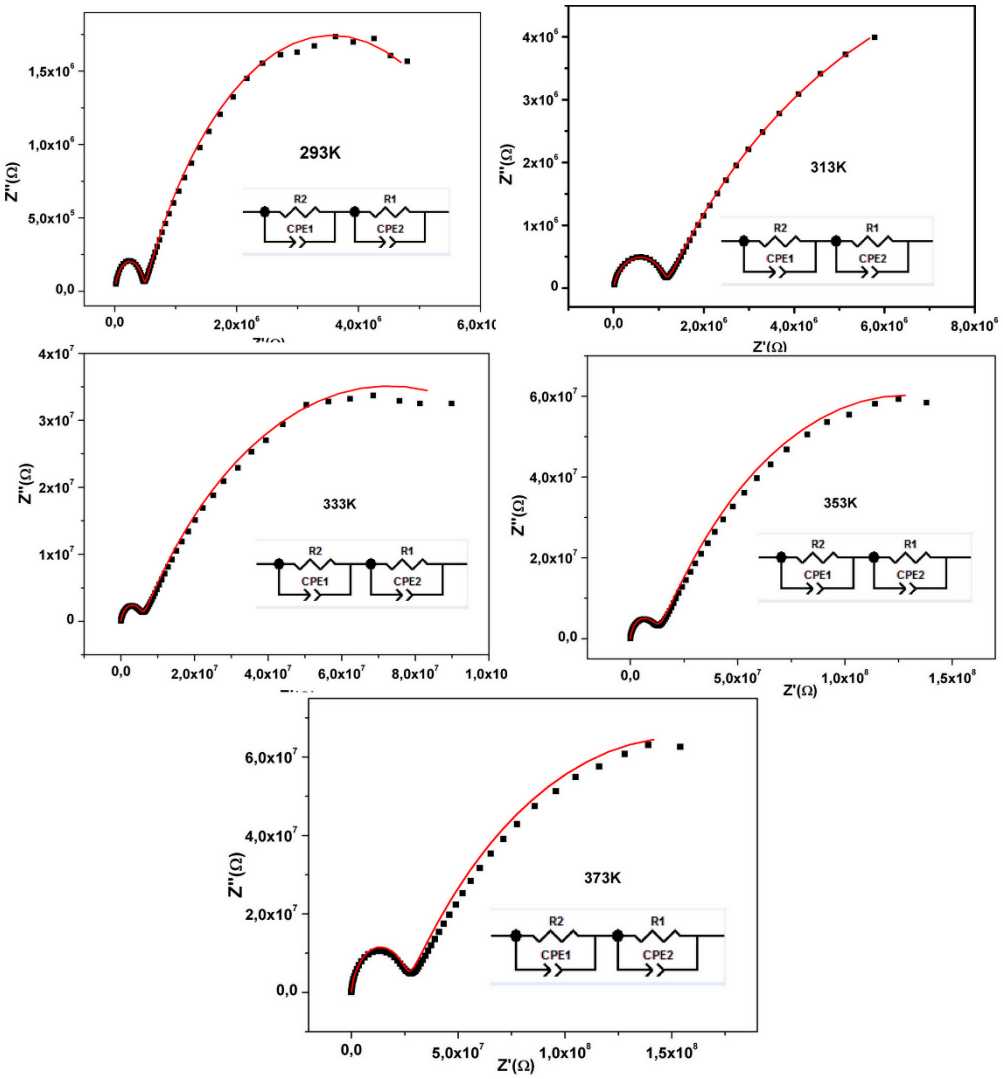

Fig.12

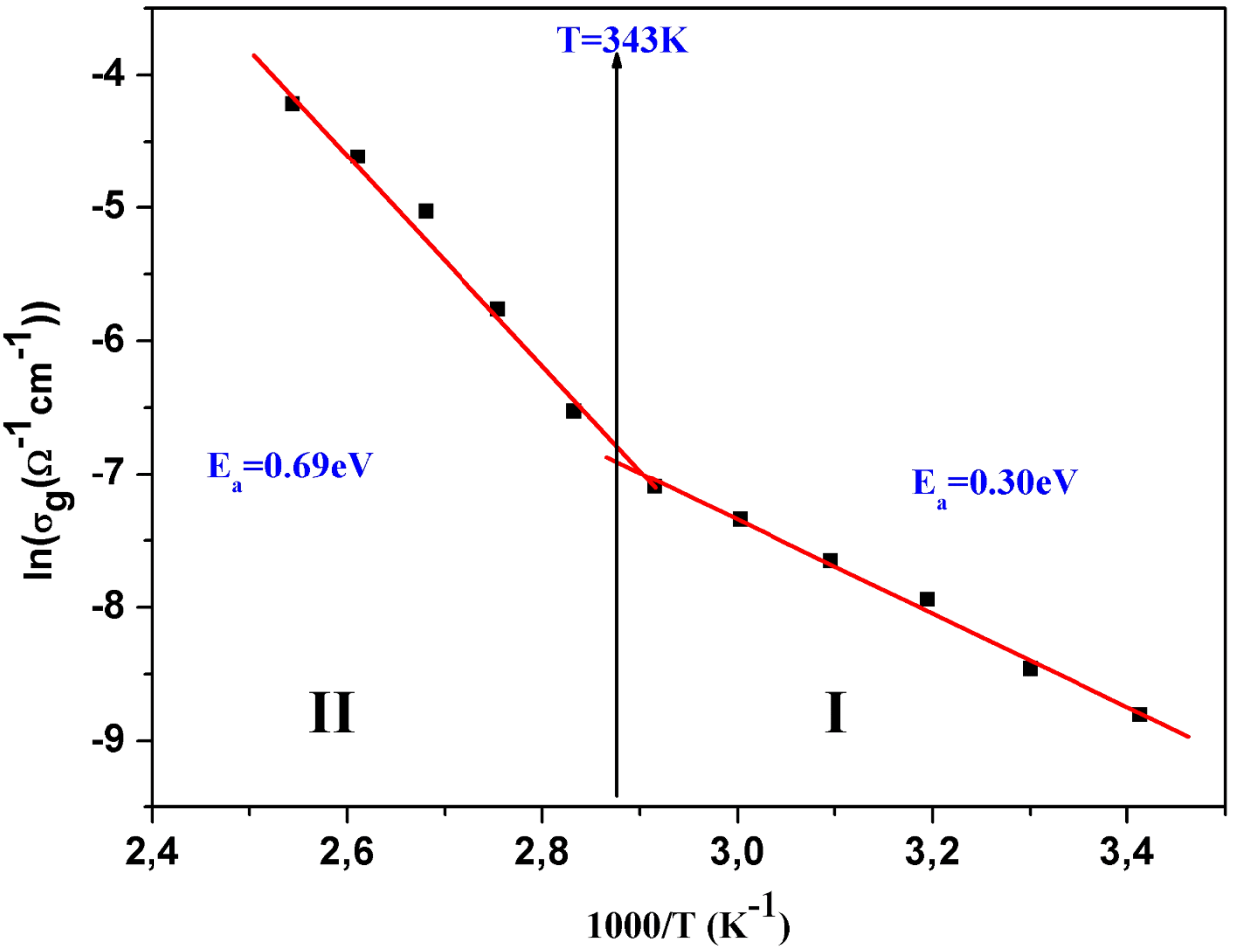
T=343K
E_a=0.69eV
E_a=0.30eV
II
I
$\ln(\sigma_g(\Omega^{-1}cm^{-1}))$
1000/T (K^{-1})
-4
-5
-6
-7
-8
-9
2,4
2,6
2,8
3,0
3,2
3,4

Fig.13

Graphical Abstract

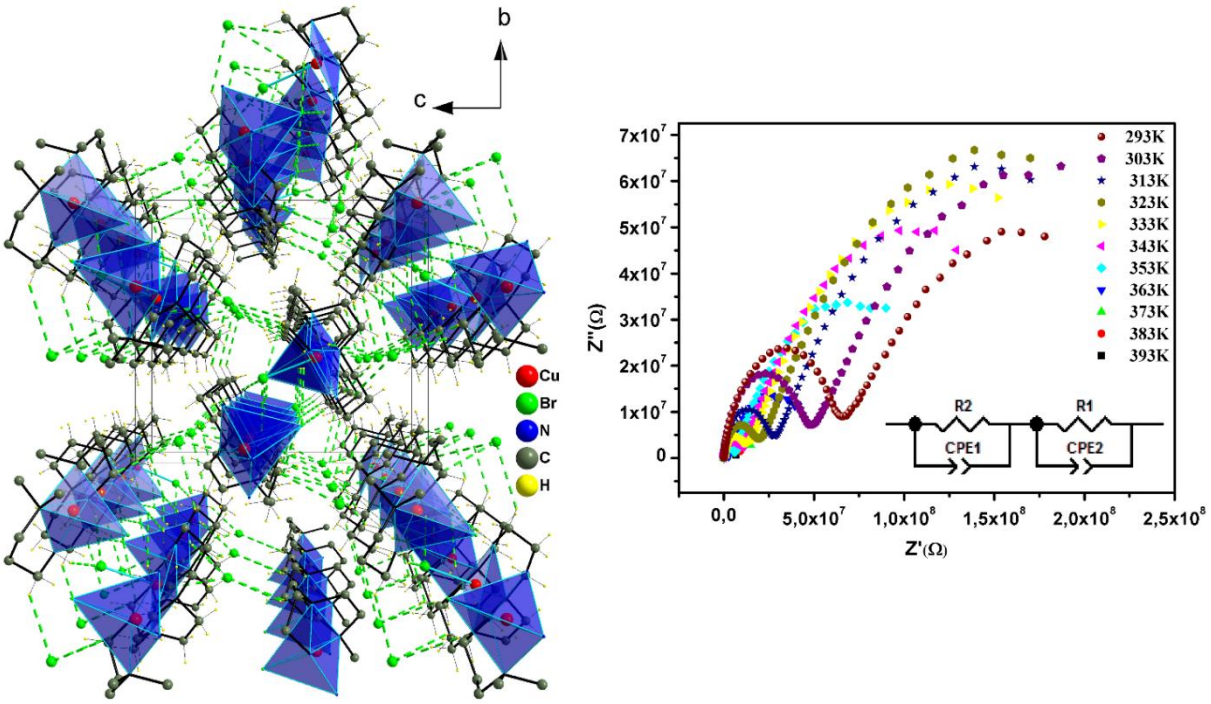

Table 1.

Table 1. Crystal data and structure refinement details for $[Cu(C_{10}H_{24}N_4)Br]Br$.

Color	Blue-violet
formula	$[Cu(C_{10}H_{24}N_4)Br]Br$
Mr ($g.mol^{-1}$)	423.68
Crystal system	Orthorhombic
Space group	$P2_12_12_1$
Temperature (K)	293(2)
a (Å)	8.3536 (1)
b (Å)	12.7161 (3)
c (Å)	14.1982 (3)
Volume($Å^3$)	1508.21 (5)
Z-space group	4
μ(mm^{-1})	6.73
Crystal size (mm^3)	0.15×0.09×0.08
F (000)	844
Diffractometer	Bruker APEX II
Radiation, λ(Å)	Mo Kα radiation, λ = 0.7107 Å
Observed reflections I > 2σ(I)	2997
R_{int}	0.032
Range of h, k, l	−10/10, -14/16, -18/16
Refined parameters	155
goodness of fit	1.16
Final R_1 and wR_2	0.029/0.056
w	$=1/[\sigma^2(F_o^2)+0.0224P^2]$ where $P = (F_o^2 + 2F_c^2)/3$
independent reflections	3589
measured reflections	10667
$\Delta\rho_{max}$, $\Delta\rho_{min}$ (e $Å^{-3}$)	0.46, -0.55
Flack parameter	-0.010(6)
CCDC no.	2060317

Table 2.

Table 2. Hydrogen-bonding geometry (Å, °) for[Cu($C_{10}H_{24}N_4$)Br]Br.

D—H···A	**D—H**	**H···A**	**D···A**	**D—H···A**
N3—H33B···Br1^{i}	0.890(8)	2.81	3.557 (4)	142
N4—H44A···Br1^{i}	0.890(8)	2.61	3.462 (4)	162
C3—H3B···Br1	0.97(9)	3.13	3.593 (5)	111
C5—H5B···Br1^{ii}	0.97(9)	3.02	3.993 (5)	177
N3—H33A···Br2	0.890(8)	2.62	3.423 (4)	150
N4—H44B···Br2	0.890(8)	2.74	3.493 (4)	143
C3—H3B···Br2^{iii}	0.97(9)	3.09	3.864 (5)	138
C7—H7B···Br2^{iv}	0.97 (9)	3.10	3.918 (5)	14
C10—H10A···Br2^{v}	0.97 (9)	3.14	3.726 (4)	120
Symmetry codes: *(i)x+1/2, −y+1/2, −z+1; (ii) x−1/2, −y+1/2, −z+1; (iii) −x+3/2, −y+1, z+1/2; (iv) −x+2, y−1/2, −z+1/2; (v) −x+5/2, −y+1, z+1/2.*				